NUMERICAL SIMULATION OF RADIATING FLOWS

A THESIS SUBMITTED TO
THE GRADUATE SCHOOL OF NATURAL AND APPLIED SCIENCES
OF
MIDDLE EAST TECHNICAL UNIVERSITY

BY

ERTAN KARAİSMAİL

IN PARTIAL FULFILLMENT OF THE REQUIREMENTS
FOR
THE DEGREE OF MASTER OF SCIENCE
IN
CHEMICAL ENGINEERING

AUGUST 2005

Approval of the Graduate School of Natural and Applied Sciences.

Prof. Dr. Canan Özgen
Director

I certify that this thesis satisfies all the requirements as a thesis for the degree of Master of Science.

Prof. Dr. Nurcan Baç
Head of Department

This is to certify that we have read this thesis and that in our opinion it is fully adequate, in scope and quality, as a thesis for the degree of Master of Science.

Prof. Dr. Faruk Arınç
Co-Supervisor

Prof. Dr. Nevin Selçuk
Supervisor

Examining Committee Members

Asst. Prof. Dr. Görkem Kırbaş	(METU, CHE)	
Prof. Dr. Nevin Selçuk	(METU, CHE)	
Prof. Dr. Faruk Arınç	(METU, ME)	
Asst. Prof. Dr. Yusuf Uludağ	(METU, CHE)	
Dr. Olcay Oymak	(MSET)	

I hereby declare that all information in this document has been obtained and presented in accordance with academic rules and ethical conduct. I also declare that, as required by these rules and conduct, I have fully cited and referenced all material and results that are not original to this work.

Name, Last name : Ertan Karaismail

Signature :

ABSTRACT

NUMERICAL SIMULATION OF RADIATING FLOWS

Karaismail, Ertan

M.Sc., Department of Chemical Engineering

Supervisor: Prof. Dr. Nevin Selçuk

Co-Supervisor: Prof. Dr. Faruk Arınç

August 2005, 81 pages

Predictive accuracy of the previously developed coupled code for the solution of the time-dependent Navier-Stokes equations in conjunction with the radiative transfer equation was first assessed by applying it to the prediction of thermally radiating, hydrodynamically developed laminar pipe flow for which the numerical solution had been reported in the literature. The effect of radiation on flow and temperature fields was demonstrated for different values of conduction to radiation ratio. It was found that the steady-state temperature predictions of the code agree well with the benchmark solution.

In an attempt to test the predictive accuracy of the coupled code for turbulent radiating flows, it was applied to fully developed turbulent flow of a hot gas through a relatively cold pipe and the results were compared with the numerical solution available in the literature. The code was found to mimic the reported steady-state temperature profiles well.

Having validated the predictive accuracy of the coupled code for steady, laminar/turbulent, radiating pipe flows, the performance of the code for transient radiating flows was tested by applying it to a test problem involving laminar/turbulent flow of carbon dioxide through a circular pipe for the simulation of simultaneous hydrodynamic and thermal development. The transient solutions for temperature, velocity and radiative energy source term fields were found to demonstrate the physically expected trends.

In order to improve the performance of the code, a parallel algorithm of the code was developed and tested against sequential code for speed up and efficiency. It was found that the same results are obtained with a reasonably high speed-up and efficiency.

Keywords: Computational Fluid Dynamics, Radiating Flows, Method of Lines, Parallel Computing

ÖZ

IŞIMALI AKIŞLARIN SAYISAL BENZETİŞİMİ

Karaismail, Ertan
Yüksek Lisans, Kimya Mühendisliği Bölümü
Tez Yöneticisi: Prof. Dr. Nevin Selçuk
Ortak Tez Yöneticisi: Prof. Dr. Faruk Arınç

Ağustos 2005, 81 sayfa

Daha önce zamana bağlı Navier-Stokes denklemlerinin, ışınım transfer denklemi ile birlikte çözümü için geliştirilmiş olan birleşik kod, ilk önce ısıl ışımalı, hidrodinamik açıdan gelişmiş kargaşasız boru akışına uygulanmış ve kodun öngörüleri literatürdeki mevcut sayısal çözümle karşılaştırılmıştır. Farklı iletim-ışınım oranları için ısıl ışınımın akış ve sıcaklık alanlarına olan etkisi incelenmiştir. Kodun yatışkın durum için ürettiği sıcak öngörülerinin, literatürdeki çözümle uyum içinde olduğu bulunmuştur.

Kodun ısıl ışımalı ve kargaşalı akışlar için ürettiği sonuçların doğruluğunu test etmek amacıyla, kod sıcak bir gazın göreceli olarak daha soğuk bir boru içindeki tam gelişmiş kargaşalı akışına uygulanmış ve sonuçlar literatürdeki mevcut sonuçlarla karşılaştırılmıştır. Kodun kargaşalı ve ışımalı akışlar için de rapor edilen yatışkın sıcaklık profillerini üretebildiği gözlemlenmiştir.

Birleşik kodun kargaşasız/kargaşalı ve ısıl ışımalı yatışkın boru akışlarında doğru sonuçlar ürettiği görüldükten sonra, kodun zamana bağlı ısıl ışınımlı akışlardaki

performansını test etmek amacıyla, kod karbon dioksitin boru içindeki zamana bağlı kargaşasız/kargaşalı akışına uygulanmış, simultane hidrodinamik ve ısıl gelişim incelenmiştir. Elde edilen zamana bağlı sıcaklık, hız ve ışınım enerji kaynak terim alanlarının fiziksel olarak beklenen davranışları gösterdiği bulunmuştur.

Kodun performansını iyileştirmek için paralel algoritması geliştirilmiş, hızlanma ve verim için seri koda karşı sınanmıştır. Aynı sonuçların yüksek hızlanma ve verimle elde edildiği bulunmuştur.

Anahtar Kelimeler: Hesaplamalı Akışkanlar Dinamiği, Işınımlı Akışlar, Çizgiler Yöntemi, Paralel Hesaplama

to my family and Nihan

ACKNOWLEDGMENTS

I wish to express my deepest gratitude to my supervisor, Prof. Dr. Nevin Selçuk for introducing me to computational fluid dynamics and providing me support, inspiration and invaluable guidance.

I also would like to show my appreciation to my co-supervisor Prof. Dr. Faruk Arınç for his support.

Special thanks go to Ahmet Bilge Uygur for his outstanding patience and help throughout this work.

Many thanks to the members of my research group for their valuable help and discussions; Dr. Tanıl Tarhan, Işıl Ayrancı, Mehmet Onur Afacan, Mehmet Kürkçü, Yusuf Göğebakan, Mehmet Ekrem Moralı and Düriye Ece Alagöz.

Finally, I would like to thank my family for their tolerance and patience, and last but not least, a special word of gratitude to Fatma Nihan Çayan, for her patience, encouragement and especially for her love.

TABLE OF CONTENTS

LIST OF TABLES

LIST OF FIGURES

LIST OF SYMBOLS

A	Perpendicular area to the main flow direction
c_p	Specific heat capacity at constant pressure, $cal/g\ K$
D	Diameter, cm
$\vec{e}_i$	Unit vector
E	Efficiency
$\vec{g}$	Gravitational acceleration, cm/s
I	Radiative intensity, $W/m^2 sr$
k	Thermal conductivity, $cal/cm\ s\ K$
k_{t^*}	Time constant, s/m
L	Dimension of the computational domain (the largest scale in the system); Length, cm
$\dot{m}$	Mass flow rate, g/s
m	Discrete direction
NR	Number of grid points in r-direction
NZ	Number of grid points in z-direction
N	Total number of grid points
N_w	Conduction-to-radiation parameter based on wall temperature
N_{ref}	Conduction-to-radiation parameter based on reference temperature
n	Normal direction
p	Static pressure, $g/cm\ s^2$, number of processor
$\hat{p}$	z-dependent component of pressure, $g/cm\ s^2$
$\tilde{p}$	r- and z-dependent component of pressure, $g/cm\ s^2$
Pe	Peclet number
Pr	Prandtl number
$\vec{q}$	Heat flux vector, w/m^2
r	Radial distance, cm
R	Universal gas constant; Radius
Re	Reynolds number
S	Speed-up
s	Distance, m

T	Temperature, K
t	Time, s
t^*	Pseudo-time variable, s
u	Instantaneous axial velocity, cm/s
$\vec{V}$	Velocity vector, cm/s
v	Instantaneous radial velocity, cm/s
$w_{m,\ell}$	Quadrature weight for ordinate m,ℓ
z	Axial distance, cm

Greek Letters

η	Direction cosines, smallest scales of motion
ε	Emissivity
θ	Angular distance, Polar angle
κ	Absorption coefficient m^{-1}
μ	Dynamic viscosity, direction cosines, $g/cm\ s$
$\vec{\nabla}$	Vector differential operator
ρ	Density, g/cm^3
$\bar{\bar{\tau}}$	Viscous momentum flux tensor
ς	Dependent variable
σ	Stefan-Boltzmann constant, W/m^2K^4
Φ	Combined momentum flux tensor, Azimuthal angle
γ	Angular redistribution term
τ_D	Optical diameter
ξ	Direction cosines
$\vec{\Omega}$	Direction of radiation intensity
Ω	Solid angle
Ω_m	Ordinate Direction

Superscripts

n	Index for time-level
ℓ	Index for a discrete direction
T	Thermal
$+$	Forward

Subscripts

0	Initial
b	Black body
i, j	Index for spatial coordinate of interest and species
int	Internal
in	Inlet
mp	Multiple processors
out	Outlet
p	Print
ref	Reference
r	r-direction; First derivative in r-direction
R	Radiation
rr	Second derivative in r-direction
rz, zr	Second derivative in r- and z- direction
sp	Single processor
$\theta\theta$	Second derivative in θ-direction
w	Wall
z	z-direction; First-derivative in z-direction
zz	Second derivative in z-direction

Abbreviations

CFD	Computational Fluid Dynamics
CPU	Central Processing Unit
CV	Control Volume
DNS	Direct Numerical Simulation
DOM	Discrete Ordinates Method
LES	Large-Eddy Simulation
MOL	Method of lines
ODE	Ordinary Differential Equation
PDE	Partial Differential Equation
PVM	Parallel Virtual Machine
RANS	Reynolds-Averaged Navier-Stokes
RTE	Radiative Transfer Equation
TVD	Time Variation Diminishing

CHAPTER 1

INTRODUCTION

Transient, turbulent, radiating flows are of great interest from the design standpoint of advanced power reactors, gas turbines, heat exchange equipment etc. Both experimental and numerical techniques aid in investigation of flows taking place in the aforementioned fields.

Experimental investigations, providing useful information regarding a particular flow field are most of the time limited due to their costly setup and relative inconvenience to parametric study.

Computational fluid dynamics (CFD), on the other hand, provides detailed information on important flow and thermal characteristics of a fluid flow with as many parameters as desired. It also takes the advantage of applicability on different geometries with ease once it has been validated with experimental data.

Numerical simulation techniques employed in CFD for turbulent flow can broadly be classified into three categories; Reynolds-Averaged Navier-Stokes simulation (RANS), large eddy simulation (LES) and direct numerical simulation (DNS). RANS simulations which are the simplest and most practical approach in use are carried out by solving time-averaged Navier-Stokes equations closed with turbulence models. The main drawback of RANS technique is that it relies on the turbulence closures which are not universal. The second level of sophistication, LES, includes the simulation of time-dependent, large-scale eddy motion. In this approach, the effects of smaller scales are included by turbulence models.

The third category, DNS, consists of solving exactly all the spatial and time scales embedded in the representative flow equations, without use of any turbulence models.

Hence it is the most accurate and straightforward technique. DNS has been a very useful tool, over the past decade, for the study of transitional and turbulent flow fields, but it also has some serious limitations. First, the use of highly accurate, high-order schemes is desirable to limit dispersion and dissipation errors. Secondly, to resolve all scales of motion, one requires a number of grid points $N \sim L/\eta$, where L is the dimension of the computational domain (the largest scale in the system) and η is the smallest scale of motion, the Kolmogorov length scale. Since the ratio is proportional to $Re^{3/4}$ for a particular direction, the number of grid points required by a three-dimensional DNS code goes like $N^3 \sim Re^{9/4}$. With this drawback in hand, it appears unlikely to apply DNS to most technological flows when one considers the fact that most of them have Reynolds numbers in tens of thousands or more which would require more grid points than computers of present day could handle. However, both use of high performance computers and efficient methods can decrease the computational time considerably. The former requirement is met by use of either supercomputers or parallel computers. The second is achieved by increasing the order of spatial discretization method, resulting in high accuracy with less grid points, and by using a highly accurate but also a stable numerical algorithm for time integration. The method of lines (MOL) that meets the latter requirement is an alternative approach for time-dependent problems. In the MOL approach, the system of partial differential equations (PDEs) is converted into an ordinary differential equation (ODE) initial value problem by discretizing the spatial derivatives together with the boundary conditions using a high-order scheme and integrating the resulting ODEs using a sophisticated ODE solver which takes the burden of time discretization and chooses the time steps in such a way that maintains the accuracy and stability of the evolving solution. The most significant advantage of MOL approach is that it has not only the simplicity of the explicit methods but also the superiority of the implicit ones unless a poor numerical method for the solution of the ODEs is employed.

1.1 Overview of the Studies

Numerous industrial applications such as combustion chambers, engines, etc. involve flow of radiatively participating gases at high temperatures. Due to design and efficiency considerations, coupled convective and radiative heat transfer in such systems has received considerable research attention. Over the past four decades much effort has been devoted to understanding of coupled convective and radiative heat transfer which can not be treated separately. The subject was studied by a number of investigators on both experimental and theoretical basis. In the earlier studies, consideration is mostly given to the mathematical formulation of the complicated nonlinear integro-differential energy equation which is very difficult to solve. Therefore, various simplifying assumptions for both flow and radiation have been frequently invoked by the researchers.

The pioneering work on coupled heat transfer was carried out by Viskanta. He [1] investigated the interaction between conduction, convection and radiation in a fully developed laminar flow of an absorbing, emitting, gray gas between two diffuse, nonblack, isothermal, parallel surfaces. The two-dimensional nonlinear integro-differential equation, namely the energy equation, was solved by an approximate solution based on the Taylor series expansion of T^4. Moreover, for two limiting cases; transparent and opaque mediums, the simplified forms of energy equation were solved and the results were compared with those of approximate solution. Calculations were carried out by assuming constant physical properties, and neglecting axial component of conduction and radiation. For a wide range of physical parameters such as optical thickness, conduction-to-radiation ratio, wall emissivities etc. the heat transfer characteristics were investigated, and it was found that the transparent and opaque approximations are very limited in their validity.

Later in several studies [2–5], the fully developed temperature profile assumption, which simplifies the integro-differential energy equation to an ordinary integro-differential equation, was used. The resultant equation which is identical in appearance to that for the combined radiation-conduction problem for the same

geometry, except for the presence of source term can be solved by the same techniques as used for combined radiation-conduction problems. This fully developed temperature profile assumption to simplify the problem has been carried over from channel flows with heat transfer by convection mode only. However, in the posterior studies Lii and Özışık [6], Liu and Thorsen [7], and Pearce and Emery [8] have found that the temperature distribution in the fluid is affected by the absorbed radiation especially for the systems where intense radiation interaction occurs. Therefore, they concluded that thermally developed temperature distribution assumption is a doubtful one. Balakrishnan and Edwards [9] compared their results for radiation and total Nusselt numbers at large distances from the entry to the results of Wassel and Edwards [5] for thermally and hydrodynamically established turbulent flow in a pipe. These authors found that maximum errors in these Nusselt numbers were 2.2 percent and 7 percent, respectively, which are quite low, corresponding to radiation-to-conduction ratio of 10.0. In order to provide a clarification for this unclear situation, and to provide an appraisal for the validity of this assumption, Chawla and Chan [10] performed a study for thermally developing Poiseuille flow with scattering. Besides findings on the effect of scattering to heat transfer, the authors observed that along the channel the Nusselt number first decreases and reaches a minimum and then increases significantly particularly at low values of conduction-to-radiation parameter and at moderate to high values of optical thicknesses. This behavior, verified also by Lii and Özışık [6] and Kurosaki [11] has not been observed in pure convection where the Nusselt number approaches an asymptotic value. Therefore, the similarity in the temperature profile appears to exist only at moderate to high values of conduction to radiation parameter.

Several studies on one-dimensional and two-dimensional radiative propagations in a fluid flowing inside the ducts exist in the literature. Among them, some [8, 10, 12–15] considered only the radial propagation whereas the others [16–28] took into account both radial and axial propagations.

Einstein [20] investigated the two-dimensional combined convective and radiative heat transfer to a uniformly absorbing gas flowing through a black circular pipe.

For the sake of simplicity axial component of conduction was neglected. The effect of various parameters of physical interest such as conduction-to-radiation ratio and gas opacity on heat transfer characteristics was reported. The results indicated that the heat transfer from the wall to the gas goes through a maximum as the opacity of the gas is increased. Thereafter, for further increases in opacity, the amount of heat transferred to the gas steadily decreases due to corresponding increase in self-shielding effect of the gas to the radiation being emitted from the pipe walls.

Nichols [29] considered the thermal entrance length problem for turbulent flow of a non-gray gas (water vapor) in an annulus. The interaction of radiation with conduction and convection was studied by assuming absorption effects based on average temperature, and gas to gas radiation was ignored in certain regions. The analysis is restricted to cases for which the radiation absorption is small compared to the convection since the solution was obtained by perturbing the solution to an equivalent problem for a non-absorbing gas. To simplify the calculations, the momentum equation was not considered, instead the axial velocity profile was determined experimentally. An analytical solution procedure was followed for the solution of energy equation. In order to estimate the radiative properties of the medium a statistical model was chosen. Analytical and experimental results were compared for the case of water vapor flowing at Reynolds numbers near 20,000 at a pressure of 3.22 atm with an inner wall temperature of 2,000 °R . A good agreement between the experimental measurements and calculated values for temperature profile and the heat transferred was found.

Later, DeSoto [30] developed an analytical procedure to investigate the coupling of radiation with the conduction and convection mechanisms in a non-isothermal, non-gray, fully developed laminar, steady gas flow in the entrance region of a tube with isothermal, black walls. Both axial and radial radiative components were included. An exponential band model was used to represent the temperature and wavelength dependence of the spectral absorption coefficients. Axial component of the heat conduction was considered negligible and constant thermophysical properties were assumed. For flux distribution trapezoidal multiple integration was employed, then a

finite difference method was used to compute temperature distribution. The calculated heat fluxes were presented for coupled problem (convection and radiation) and Graetz problem (convection only). The results showed that although the axial radiative flux component is large at the entrance, it decreases rather abruptly as the flow proceeds only a short distance into the tube and its effect thereafter on temperature distribution becomes negligible.

Pearce and Emery [8] have utilized the conclusion of DeSoto by considering the propagation of radiation as one-dimensional in their investigation of the heat transfer by coupled thermal radiation and laminar forced convection to an absorbing fluid in the entrance region of a black-walled, isothermal, circular pipe. The fluid enters the pipe with fully developed or uniform velocity profiles. The medium was treated as both gray and non-gray. The two-dimensional continuity, momentum and energy equations were approximated by finite difference approach for a rectangular non-uniform mesh. As non-gray radiation model, the box model was chosen and applied to carbon monoxide and carbon dioxide and calculations additionally include the effects of variable transport properties and variable density, which is not considered for the calculations of gray case. The non-gray results obtained by box model were compared with those of wide-band model. It was found that when strong interaction between radiation and convection exists, the coupled solution becomes a must and that the effects of radiation is more important when the fluid is heated than when it is cooled.

Later, Echigo *et al.* [18] made a further investigation which brought together the previously scattered knowledge on the use of one-dimensional and two-dimensional treatment of radiation propagation. Although there were studies [20, 30] in which the radiative heat transfer was taken into account as being two-dimensional, they lack of the generality and precision due to the constraints in numerical procedure and the analytical methods used and further the propagation of the thermal radiation into the region upstream is not considered at all. For this purpose, as a physical system the authors have chosen a circular pipe -with an abrupt change in wall temperature- through which laminar flow of an absorbing and emitting medium takes place. The authors solved the problem assuming the flow is fully developed and

taking the radiation propagation as two-dimensional. The results have shown that one-dimensional treatment of radiation underestimates both its contribution and the heat transfer characteristics near the entrance of heating section in the region downstream.

In a recent study Baek *et al.* [31] examined the thermally developing but hydrodynamically developed Poiseuille flow of an absorbing, emitting and scattering medium through a pipe with black wall. The two-dimensional radiation was solved by using discrete ordinates method (DOM). The S_4 order of approximation has been adopted. The energy equation was discretized by finite difference approximations on a 21×21 uniform grid system. Authors validated their predictions against numerical solution of Echigo *et al.* [18]. With this advantage, they reported the effect of optical thickness of the medium and the conduction-to-radiation ratio on heat transfer characteristics.

All of the studies except [29] mentioned so far have been applied to laminar flows. However, there are a number of studies [13, 28, 32–36] in which consideration is given to turbulent flows. One of them is the study of Landram *et al.* [33] in which the heat transfer in fully developed turbulent flow of a radiating optically thin absorbing emitting gas in a circular tube was determined. The radiation problem was formulated in terms of the Planck mean and the modified Planck mean coefficients. Only radiative properties were allowed to vary with temperature. The temperature profiles and the Nusselt number distribution were reported. Later, Habib and Greif [37] performed both an experimental and a theoretical study on the same subject except optically thin conditions. In the theoretical part of the study, the gas was considered as non-gray and an approximate formulation was employed for the determination of radiative transport. In experimental part, air and carbon dioxide were studied respectively. The results were presented in terms of temperature profiles and comparisons were made. A good agreement between results of theoretical and experimental studies was found. As an extension to this study Chiba and Greif [34] made a research for water vapor using the same experimental set-up.

Balakrishnan and Edwards [9] studied the thermal development in a non-gray medium

(water vapor and carbon dioxide). The momentum equation was solved by numerical integration and implicit finite difference technique was used for the solution of integro-differential energy equation. For both laminar and turbulent flows, findings on total and radiative Nusselt numbers and dimensionless bulk temperature were reported. Also a correlation for average Nusselt number for turbulent duct flow of radiating medium was suggested.

Wassel *et al.* [38] later, solved the non-gray radiation and thermal diffusion in a thermally and hydrodynamically established laminar or turbulent pipe flow with uniform internal heat generation. Solutions were presented for radiative and convective Nusselt number as a function of radiation parameters such as radiation-to-conduction ratio, optical thickness and turbulent Reynolds number. The radiative Nusselt number was found to increase about linearly with radiation-to-conduction ratio and linearly with optical thickness at small optical thicknesses but approximately logarithmically at large optical thicknesses.

Tsou and Kang [32] focused on the situation where turbulent convection and thermal radiation act simultaneously in the gas flow. The physical system used is very similar to the one used in the study of Echigo *et al.* [18]. The thermophysical properties were assumed to be constant. The black plug approximation at the ends of the duct was not used. For the radiative transfer the Eddington's approximation was used and the problem was solved using Green's function. The results were presented for temperature profile and Nusselt number. It was found that for strong radiation not only the axial component of radiation but also the axial heat diffusion must be accounted for.

An analysis of heat transfer for laminar or turbulent fully developed flow with developing temperature profiles of a radiatively participating gas through a black-walled circular tube was made by Smith *et al.* [21] for prescribed wall temperature and heat flux distributions. The medium was taken as theoretical (gray) or real (non-gray) gas. The analysis showed that the magnitude of the wall heat flux for specified wall temperatures for a real gas decreases with axial distance but increases near the

outlet due to radiant exchange with the outlet surface. Wall heat flux with radiation was found to be larger than that without radiation for the same values of the system parameters. The gas temperature profile is more uniform for turbulent flow than for laminar flow under either specified wall temperature or heat flux distributions. The Nusselt numbers with gaseous radiation are higher by about a factor of ten than those without radiation for the same values of the system parameters.

One of the most detailed study especially in terms of flow was carried out by Schuler and Campo [23]. In the study the interactive heat transfer problem involving turbulent forced convection and radiation in the thermal development region of a gray gas pipe flow was analyzed. The authors assumed that the fluid enters the pipe with a fully developed turbulent velocity profile. The turbulence model adopted for the velocity profile involves the solution of one differential equation for the kinetic energy of turbulence ((*K*, *L*) model of turbulence). Using the gray gas assumption, the radiation contribution is modeled by a differential method, the so-called method of moments. Although the importance of the two-dimensional solution of thermal radiation was emphasized by Echigo *et al.* [18], in this study Schuler and Campo accounted for only the radial propagation of radiation and supported their approach with the expectancy of much smaller upstream radiation in turbulent flow regimes. With the new formulation of the governing equations a coupled system consisting of a partial differential equation for temperature, namely energy equation and an ordinary differential equation for the irradiation formed. The former was solved by a hybrid methodology (MOLCV) utilizing the method of lines (MOL) solution in conjunction with a control volume (CV) discretization in the radial direction only. Similarly, the latter was discretized by control volumes too. The resulting initial value problem was solved by integrating numerically with Runge-Kutta-Fehlberg scheme. The predictions of the proposed solution method (MOLCV) was found to agree well with the other numerical results available in the literature.

Nakra and Smith [39] studied the interaction of radiative transfer with convective transfer for slug flow of an absorbing emitting gas in a circular tube with isothermal walls. The zone method was utilized for radiation exchange calculations. Gas

properties were evaluated from the weighted sum of gray gases model and for the solution of energy balance an iterative procedure was employed. Axial temperature distribution as well as local and overall wall heat transfer rates were presented for different values of several governing parameters such as Boltzman and Stanton numbers, inlet and wall temperatures, length to diameter ratio.

Besides the above mentioned studies, there has been a number of studies [10, 13, 15, 19, 35, 40] dealing with the interaction between convection and radiation in gas-particulate systems.

Among them, Chawla and Chan [10] examined the thermally developing Poiseuille flow between two infinite parallel plates. The fluid was absorbing, emitting and isotropically scattering. Gray gas, and constant thermophysical properties assumptions were invoked. To solve the problem spline collocation method was used. The analysis revealed that scattering tends to decrease the radiation component as well as convective component of heat transfer significantly at moderate to low values of optical thickness, whereas at high values of optical thickness, the effect of scattering on the radiation component appears to be less pronounced, and the effect on the convective component remains undiminished. The net effect of scattering was found to decrease the total Nusselt number. As an important feature of the interaction between radiation and convection it was observed that total Nusselt number appears to increase significantly downstream of the location of its minimum, particularly in the presence of intense radiation.

Azad and Modest [13] extended the previous two works done by De Soto [30] and Chawla and Chan [10] by including the diffuse reflection and the effects of linear-anisotropic scattering effects. One-dimensional radiation propagation was considered and axial conduction was excluded. The governing differential equations were solved numerically by an implicit finite difference method with an iterative procedure. The results have shown that no fully developed temperature profile could be expected to form which has already been stated by Chawla and Chan [10]. Tabanfar and Modest [15] extended the interaction of thermal radiation with conduction and convection for

turbulent fluid flow to include non-gray effects, but with black walls and constant surface heat flux using an exact treatment of radiative flux. Exponential wide band model was used to predict radiative properties.

Yener and Özışık [40] investigated simultaneous radiation and forced convection for an absorbing, emitting and isotropically scattering thermally developing turbulent flow of a gray fluid through a parallel-plate channel with reflecting isothermal walls. The radiative transfer was solved employing Galerkin's method which includes diffuse reflection effects also. Assuming constant thermophysical properties for the fluid and excluding axial conduction as well as axial radiation, the energy equation was solved by an iterative procedure. Results were presented for a Reynolds number of 100,000 and a Prandtl number of 1.0. From the results it was observed that as the reflectivity approaches unity, the Nusselt number approaches that of nonradiating flows.

Huang and Lin [19] studied the interaction of thermal radiation with laminar forced convection in thermally developing, circular pipe flow. Two-dimensional radiation model was included for absorbing, emitting and isotropically scattering gray fluid bounded by a heated wall having a sudden change in temperature. The contribution of thermal radiation was obtained by solving the exact integral equations for the source function and boundary intensity with an iteration method. The governing energy equation was solved numerically by the fully implicit finite difference method with an iterative procedure. The results indicated that the axial radiation effect becomes significant at small conduction-to-radiation parameter and/or higher wall-to-inlet temperature ratio.

Krishnaprakas *et al.* [35] investigated steady-state, combined forced convection, and radiation heat transfer in an absorbing, emitting and anisotropically scattering gray fluid flowing through a circular tube. The flow was assumed to be hydrodynamically fully developed and turbulent. For turbulence modeling eddy diffusivity concept was used. Diffusive and radiative heat transfer in axial direction was neglected, and the energy equation was solved by Crank-Nicolson method. Discrete ordinates method

(DOM) with S_6 order of approximation was used for radiative transfer calculations. The calculated Nusselt numbers were presented and it was found that the minimum value of local Nusselt number shifts towards inlet as the radiative contribution increases. This was attributed to the continuous reduction in convective heat flux and augmentation of radiative flux as it moves away from the inlet. Also the presence of anisotropy was found to affect the heat transfer significantly for low values of conduction-to-radiation ratio and high values of scattering albedo.

An analysis is made by Franca and Goldstein Jr. [28] on the heat transfer in the fully developed turbulent flow of carbon dioxide, water vapor and nitrogen mixture through a circular tube whose outer surface is covered by nonideal insulation. For the situation they considered, it was found that three basic parameters; (1) the gas inlet temperature, (2) the tube inner diameter, and (3) the Reynolds number affect the coupled heat transfer in the gas flow. The radiation processes was affected mainly by the first two parameters in such a way that the larger the gas inlet temperature and the tube inner diameter, the more significant the effect of the radiation process. The convection process depends basically on the Reynolds number, becoming more important as this parameter increases.

One of the most detailed and realistic analysis on combined convection and radiation in a parallel plate channel has been carried out by Soufiani and Taine [41]. In this study, flow and thermal development in a channel was taken into account, and temperature-dependent thermophysical properties were used. Radiative properties were calculated by random-statistical narrow band model with 25 cm^{-1} resolution and radiative transfer equation was solved using the Curtis-Godson approximation. The continuity, momentum and energy equations are solved simultaneously. Calculations were reported for water vapor-air mixtures between two parallel walls of constant gray emissivity. The Reynolds number was set to 2500. Both heating and cooling of the fluid were considered. The results showed that the temperature field is significantly modified due to presence of radiation. A uniform temperature distribution in the central region of the channel was observed and this was attributed to sufficiently large gas opacity and gas-to-gas radiation exchange. Near the thermal entry, the wall

temperature gradient was found to be greater than that obtained for pure convection, but the opposite behavior was observed towards the outlet. A radiative boundary layer was observed in the viscinity the wall, and inside this layer, the strong temperature gradient causes the sign of the radiative flux divergence to become the opposite of that obtained near the center of the channel. Coupled convective and radiative heat transfer in the case of carbon dioxide and water vapor laminar flows has been studied both experimentally and theoretically [42]. A very good agreement between measured and predicted temperature profiles has been obtained, particularly in the case of carbon dioxide flows.

In a recent study, Soufiani and Taine [42] studied coupled radiative and convective heat transfer experimentally and theoretically in the case of carbon dioxide and water vapor laminar flows through a channel with uniform wall temperature and rectangular cross-section. The spectral radiative properties of the flowing gas were calculated by using a statistical narrow-band model. The two-dimensional governing flow and energy equations were solved simultaneously in order to account for the temperature dependencies of density and viscosity. An implicit finite difference scheme was used for the solution. A very good agreement between the measured and calculated temperature profiles was obtained.

Later, a similar analysis was performed by Sediki *et al.* [43] for the flow carbon dioxide and water vapor through a cylindrical duct. The duct under consideration had a jump in wall temperature. The propagation of radiation was considered as both one-dimensional and two-dimensional. Preheating or precooling of the gas before the temperature jump was allowed through the axial component of radiative flux. Narrow-band correlated-k model and absorption distribution function (ADF) model were used to predict the radiative properties of flowing medium. A discrete direction method was employed to predict radiative transfer, and an implicit finite difference technique was used to solve flow equations. The analysis revealed that the effects of the radiative axial component should be accounted for when the difference between the wall and bulk temperature is significant.

1.2 Principle Objective of the Present Study

Most of the previous studies on thermally radiating internal flows have been reviewed in the preceding section. The review reveals that most of these studies focused on the solution methods of the energy and radiative transfer equations for laminar flows, and that the fundamental difficulties associated with the accurate solution of flow field were by-passed by assuming hydrodynamically developed conditions. Furthermore, variation of thermophysical properties such as density and viscosity with temperature was not taken into consideration in the majority of these studies. However, an accurate analysis necessitates the solution of time dependent Navier-Stokes equation in conjunction with the radiative transfer equation (RTE) as well as utilization of temperature-dependent thermophysical properties.

In an attempt to achieve this objective a novel DNS based CFD code developed by Selçuk and her co-workers for two-dimensional internal flows in regular and complex geometries was coupled with a radiation code developed by the same authors using the methodology outlined in [44]. The CFD code uses the MOL approach in conjunction with a higher-order adaptive scheme and a parabolic pressure algorithm for the simulation of time-dependent incompressible separated internal flows in complex geometries using general curvilinear coordinate system. The requirement of high performance computing was met by developing an efficient parallel algorithm for the code. Predictive accuracies and performances of both sequential and parallel codes were assessed on various laminar and turbulent isothermal/non-isothermal flow problems by validating its predictions against either measurements or numerical results available in the literature [44–51]. Favorable comparisons were obtained on these non-reacting flow problems. Comparisons also showed that the flow field predicted by parallel code agreed well with those of serial code at considerably less execution times.

Radiation code, on the other hand, is based on MOL solution of discrete ordinates method (DOM). Predictive accuracy of the code was previously validated against exact solution, Monte Carlo and zone method solutions as well as the measurements

on a wide range of one-dimensional and multi-dimensional problems in Cartesian coordinates including absorbing, emitting strongly anisotropically scattering, gray media bounded by gray, diffuse walls [52–54]. Recently, the method was applied to axisymmetric cylindrical enclosures containing absorbing, emitting, gray medium and its predictions were validated against exact solutions and measurements [55]. The method was also found to be successfully applicable to solution of transient radiative transfer problems [56].

The performance of the above-mentioned coupled code was tested on a laminar, axisymmetric, hydrodynamically developed flow of a gray, absorbing, emitting fluid in a heated pipe. Temperature profiles predicted by the coupled code were validated against steady-state solutions available in the literature. Favorable comparisons showed the predicted accuracy and reliability of the coupling strategy employed.

Depending on the relative importance of radiation to conduction, the heat transfer characteristics in high-temperature practical applications may vary to a great extent. This may point to further investigation of effect of different conduction to radiation ratios on temperature fields. Furthermore, although the studies on laminar radiating flows aid in understanding some aspects of more complicated flow scenarios, simulation of turbulent radiating flows is of greater importance in the sense that they are involved in almost all practical high-temperature systems. Hence the objective of this study has been to:

- investigate the effect of radiation on temperature fields by using the coupled code,
- apply the coupled code to the prediction of the turbulent, radiating axisymmetric flows, and validate its predictions against available numerical predictions,
- parallelize the coupled code and evaluate its performance with respect to accuracy and central processing unit (CPU) time.

CHAPTER 2

THE GOVERNING EQUATIONS

2.1 General

In this chapter, the governing equations of fluid dynamics (i.e. fluid mechanics and heat transfer) and radiative transfer are described.

The fundamental equations describing the non-isothermal flow of fluids in the absence of chemical reaction or mass diffusion are based on three physical conservation laws:

- Conservation of mass,
- Conservation of momentum,
- Conservation of energy.

Application of conservation of mass to a fluid element within a flowing fluid yields equation of continuity. The law of conservation of momentum, which stems from Newton's second law results in equation of motion or momentum equation. The application of conservation law of energy which is actually the first law of thermodynamics results in equation of energy. The detailed derivation of the conservation equations can be found elsewhere [57].

In flow applications where radiation and convection are co-principal heat transfer mechanisms, coupling between these different modes of energy transfer is unavoidable and consequently the governing equations are interlinked. This link is established through radiative source term appearing in the energy equation.

2.2 The Governing Equations of Fluid Dynamics

In the case of transient incompressible non-isothermal radiating flows , the governing equations of fluid dynamics can be written in vectorial form as follows;

continuity;

$$\vec{\nabla} \cdot \vec{V} = 0, \tag{2.1}$$

momentum;

$$\rho \left(\frac{\partial \vec{V}}{\partial t} + \vec{V} \cdot \vec{\nabla} \vec{V} \right) = -\vec{\nabla} p - \vec{\nabla} \cdot \bar{\bar{\tau}} + \rho \vec{g}, \tag{2.2}$$

energy;

$$\rho c_p \left(\frac{\partial T}{\partial t} + \vec{V} \cdot \vec{\nabla} T \right) = \vec{\nabla} \cdot \left(k \vec{\nabla} T \right) - \vec{\nabla} \cdot \vec{q_R}, \tag{2.3}$$

where $\vec{V}$ is the velocity vector, p is the static pressure, $\bar{\bar{\tau}}$ is the stress tensor, $\vec{g}$ is the gravitational acceleration, T is the temperature, $\vec{q_R}$ is the radiative source term and finally c_p and k are the specific heat capacity and the thermal conductivity of the fluid, respectively.

2.2.1 Governing Equations in Cylindrical Coordinates

The 2D incompressible Navier-Stokes equations written in cylindrical coordinates together with the energy equation in the absence of viscous dissipation and heat generation terms are

continuity;

$$\frac{\partial u}{\partial z} + \frac{\partial v}{\partial r} + \frac{v}{r} = 0, \tag{2.4}$$

z-momentum;

$$\rho \left(\frac{\partial u}{\partial t} + u \frac{\partial u}{\partial z} + v \frac{\partial u}{\partial r} \right) = -\frac{\partial p}{\partial z} - \left(\frac{1}{r} \frac{\partial}{\partial r} (r \tau_{rz}) + \frac{\partial \tau_{zz}}{\partial z} \right) + \rho g_z, \tag{2.5}$$

r-momentum;

$$\rho \left(\frac{\partial v}{\partial t} + u \frac{\partial v}{\partial z} + v \frac{\partial v}{\partial r} \right) = -\frac{\partial p}{\partial r} - \left(\frac{1}{r} \frac{\partial}{\partial r} (r \tau_{rr}) + \frac{\partial \tau_{rz}}{\partial z} - \frac{1}{r} \tau_{\theta\theta} \right) + \rho g_r, \tag{2.6}$$

where for Newtonian fluids

$$\tau_{rr} = -\mu\left(2\frac{\partial v}{\partial r}\right), \tag{2.7}$$

$$\tau_{zz} = -\mu\left(2\frac{\partial u}{\partial z}\right), \tag{2.8}$$

$$\tau_{\theta\theta} = -\mu\left(2\frac{v}{r}\right), \tag{2.9}$$

$$\tau_{rz} = \tau_{zr} = -\mu\left(\frac{\partial u}{\partial r} + \frac{\partial v}{\partial z}\right), \tag{2.10}$$

energy;

$$\rho c_p\left(\frac{\partial T}{\partial t} + u\frac{\partial T}{\partial z} + v\frac{\partial T}{\partial r}\right) = -\left(\frac{1}{r}\frac{\partial}{\partial r}(rq_r) + \frac{\partial q_z}{\partial z}\right) - \vec{\nabla}\cdot\vec{q}_R, \tag{2.11}$$

where

$$q_r = -k\frac{\partial T}{\partial r}, \tag{2.12}$$

$$q_z = -k\frac{\partial T}{\partial z}. \tag{2.13}$$

Substitution of Equations 2.7 to 2.10 into Equations 2.5 and 2.6, and of Equations 2.12 and 2.13 into Equation 2.11 yield

z-momentum;

$$\begin{aligned}\frac{\partial u}{\partial t} + u\frac{\partial u}{\partial z} + v\frac{\partial u}{\partial r} = &- \frac{1}{\rho}\frac{\partial p}{\partial z} + \frac{\mu}{\rho}\left(\frac{\partial^2 u}{\partial r^2} + \frac{1}{r}\frac{\partial u}{\partial r} + \frac{\partial^2 u}{\partial z^2}\right)\\ &+ \frac{1}{\rho}\left(\frac{\partial u}{\partial r} + \frac{\partial v}{\partial z}\right)\frac{\partial \mu}{\partial r} + \frac{2}{\rho}\left(\frac{\partial u}{\partial z}\right)\frac{\partial \mu}{\partial z} + g_z,\end{aligned} \tag{2.14}$$

r-momentum;

$$\begin{aligned}\frac{\partial v}{\partial t} + u\frac{\partial v}{\partial z} + v\frac{\partial v}{\partial r} = &- \frac{1}{\rho}\frac{\partial p}{\partial r} + \frac{\mu}{\rho}\left(\frac{\partial^2 v}{\partial r^2} + \frac{1}{r}\frac{\partial v}{\partial r} - \frac{v}{r^2} + \frac{\partial^2 v}{\partial z^2}\right)\\ &+ \frac{2}{\rho}\left(\frac{\partial v}{\partial r}\right)\frac{\partial \mu}{\partial r} + \frac{1}{\rho}\left(\frac{\partial u}{\partial r} + \frac{\partial v}{\partial z}\right)\frac{\partial \mu}{\partial z} + g_r,\end{aligned} \tag{2.15}$$

energy;

$$\begin{aligned}\frac{\partial T}{\partial t} + u\frac{\partial T}{\partial z} + v\frac{\partial T}{\partial r} = &\frac{k}{\rho c_p}\left(\frac{\partial^2 T}{\partial r^2} + \frac{1}{r}\frac{\partial T}{\partial r} + \frac{\partial^2 T}{\partial z^2}\right)\\ &+ \frac{1}{\rho c_p}\left(\frac{\partial T}{\partial r}\right)\frac{\partial k}{\partial r} + \frac{1}{\rho c_p}\left(\frac{\partial T}{\partial z}\right)\frac{\partial k}{\partial z} - \frac{\vec{\nabla}\cdot\vec{q}_R}{\rho c_p}.\end{aligned} \tag{2.16}$$

2.2.2 Initial and Boundary Conditions

Initial and boundary conditions define the problem under consideration and therefore constitute an essential part of the computation.

For flows that are statistically steady, the initial conditions are relatively unimportant. Usually, they may consist of large amplitude perturbations superposed on a realistic mean flow, or of a fully developed flow in a similar configuration.Typically, the flow is allowed to develop in time until a steady state is reached. For transient problems, more care should be given to the assignment of initial conditions, and physically correct and reasonably accurate initial conditions must be provided.

There are generally five different types of boundaries which will occur in internal flows. These are solid surfaces, symmetry, periodic, inflow and outflow boundaries.

It is common practice to impose no-slip $(u = 0)$ and no-throughflow $(v = 0)$ conditions while treating stationary solid surfaces. For the energy equation generally, either a wall temperature, or adiabatic wall condition, or Newton's law of cooling is specified at the surface.In the present study, the wall temperature was kept constant.

For systems where the configuration and domain of solution is symmetrical, the axis of symmetry can be treated as a boundary. In such cases, no flow is permitted to cross the boundary $(v = 0)$ and all gradients normal to the boundary are set equal to zero $\left(\frac{\partial u}{\partial n} = \frac{\partial T}{\partial n} = 0\right)$ where n denotes the direction normal to the centerline.In dealing with the cylindrical coordinate system, the symmetry boundary condition constitutes a singularity at the symmetry axis $(r = 0)$, since the terms $\frac{1}{r}\frac{\partial u}{\partial r}$ and $\frac{1}{r}\frac{\partial T}{\partial r}$ appearing in Equations 2.14, and 2.16 are indeterminate at the center $(r = 0)$. It should be noted that the denominators of these terms are zero (from $\frac{1}{r}$), but the numerators are also zero (from the boundary conditions). This bottleneck can be alleviated by applying L' Hôpital's rule; differentiating the numerator and denominator with respect to r, i.e.,

$$\lim_{r\to 0} \frac{1}{r}\frac{\partial u}{\partial r} = \frac{\partial^2 u}{\partial r^2}, \qquad \lim_{r\to 0} \frac{1}{r}\frac{\partial T}{\partial r} = \frac{\partial^2 T}{\partial r^2}. \tag{2.17}$$

Thus, the terms $\frac{1}{r}\frac{\partial u}{\partial r}$ and $\frac{1}{r}\frac{\partial T}{\partial r}$ in the governing equations take the form $\frac{\partial^2 u}{\partial r^2}$ and $\frac{\partial^2 T}{\partial r^2}$, respectively at the center $(r = 0)$. It should be pointed out that since time-independent

Dirichlet type boundary condition $(v = 0)$ is used for the radial component of the velocity vector, there is no need to solve Equation 2.15 along the centerline.

The formulation of inflow and outflow boundary conditions continues to be one of the most difficult tasks in the numerical simulation of internal flows. Ideally it would be desirable to apply boundary conditions at upstream infinity and downstream infinity where all of the flow properties are known. However, memory capacities of even the most modern high speed computers restrict placement of computational boundaries to immediately upstream and downstream of the region of interest. For flow systems with rather short length, the implementation of the fully developed condition is not appropriate, since that kind of boundary condition is generally used for internal flow systems with considerably long length. Therefore, in the case of dealing with flow systems with short length, generally the so-called soft boundary condition [58, 59], which requires the second order streamwise derivatives to vanish, is used.

2.3 The Governing Equations of Radiative Transfer

The propagation of radiation in a participating medium is governed by the radiative transfer equation (RTE) which is derived by drawing up a balance on the flux of radiant energy in specified direction through a small volume element. The details of derivation can be found elsewhere [60–62]. The RTE for absorbing, emitting gray medium can be written in the form

$$\frac{dI}{ds} = (\vec{\Omega} \cdot \vec{\nabla}) I(\vec{r}, \vec{\Omega}) = -\kappa(\vec{r}) I(\vec{r}, \vec{\Omega}) + \kappa(\vec{r}) I_b(\vec{r}) \tag{2.18}$$

where $I(\vec{r}, \vec{\Omega})$ is the radiation intensity at position $\vec{r}$ in the direction $\vec{\Omega}$ defined as the quantity of radiant energy passing in the specified direction Ω along a path s, per unit solid angle Ω about the direction $\vec{\Omega}$, per unit area normal to the direction of travel and per unit time. $\kappa(\vec{r})$ is the absorpion coefficient of medium and $I_b(\vec{r})$ $(\equiv \sigma\, T^4(\vec{r})/\pi)$ is the black body radiation intensity at the temperature of the medium. The expression on the left hand-side is the gradient of the intensity in the specified direction $\vec{\Omega}$. The two terms on the right hand-side represent the changes in intensity due to absorption and emission, respectively.

2.3.1 Radiative Transfer Equation in Cylindrical Coordinates

In axisymmetric cylindrical geometry (r,z), the directional derivative of radiation intensity can be expressed as [61]

$$\frac{dI}{ds} = \frac{\partial I}{\partial r}\frac{dr}{ds} + \frac{\partial I}{\partial \phi}\frac{d\phi}{ds} + \frac{\partial I}{\partial z}\frac{dz}{ds} \tag{2.19}$$

where

$$\frac{dr}{ds} = \vec{\Omega}.\vec{e}_r = \mu \tag{2.20}$$

$$\frac{d\phi}{ds} = \vec{\Omega}.\vec{e}_{\theta c} = -\frac{\eta}{r} \tag{2.21}$$

$$\frac{dz}{ds} = \vec{\Omega}.\vec{e}_z = \xi \tag{2.22}$$

In Equations 2.20, 2.21, 2.22, $\vec{e}_r$, $\vec{e}_{\theta c}$,$\vec{e}_z$ are unit vectors and $\mu = sin\theta cos\phi$, $\eta = sin\theta sin\phi$, $\xi = cos\theta$ are direction cosines in r, θ_c and z directions, respectively. (See Figure 2.1)

Hence, RTE in axisymmetric cylindrical coordinates can be written as

$$\frac{dI}{ds} = \mu\frac{\partial I}{\partial r} - \frac{\eta}{r}\frac{\partial I}{\partial \phi} + \xi\frac{\partial I}{\partial z} = -\kappa I + \kappa I_b \tag{2.23}$$

the directional derivative (d/ds) is written in the so-called conservation form to assure that approximation to the RTE retain the conservation properties. Mathematically it means that upon multiplying the differential equation by a volume element, the resulting coefficient of any differential term does not contain the variable of differentiation. Equation 2.23 is not yet in conservative form, since the coefficient of $\frac{\partial I}{\partial \phi}$ is η/r and $\eta = sin\theta sin\phi$. This difficulty is easily remedied by adding and subtracting a term,$\frac{\mu}{r}I$.

Hence in conservative form RTE in axisymmetric cylindrical coordinates takes the following form

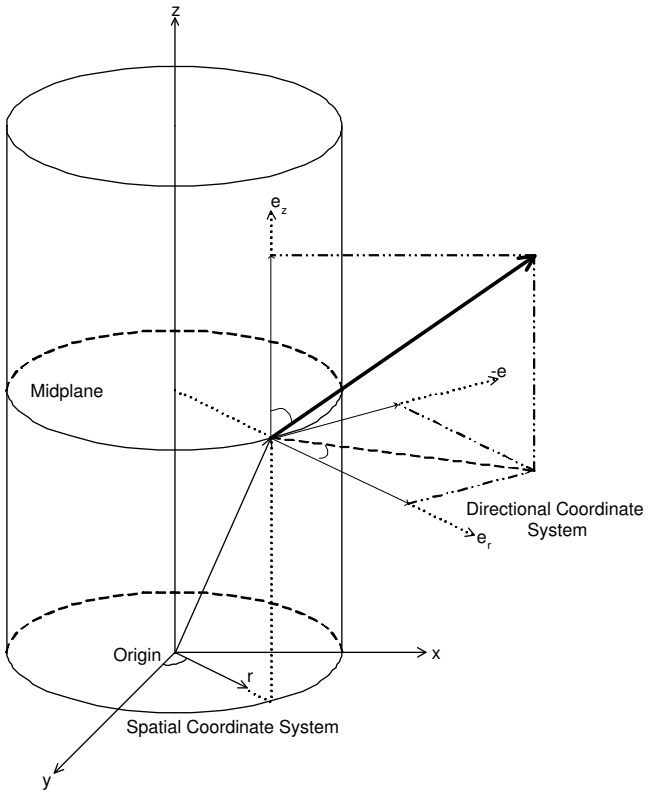

Figure 2.1: Cylindrical space-angle coordinate system in three dimensions

$$\frac{dI}{ds} = \frac{\mu}{r}\frac{\partial(rI)}{\partial r} - \frac{1}{r}\frac{\partial(\eta I)}{\partial \phi} + \xi\frac{\partial I}{\partial z} = -\kappa I + \kappa I_b \tag{2.24}$$

2.3.2 Boundary Conditions

If the surface bounding the medium is gray with specified temperature distribution, and emits and reflects diffusely then the radiative boundary condition for Equation 2.18 is given by

$$I(\vec{r_w}, \vec{\Omega}) = \varepsilon_w I_b(\vec{r_w}) + \frac{(1-\varepsilon_w)}{\pi}\int_{\vec{n_w}\cdot\vec{\Omega}'} |\vec{n_w}\cdot\vec{\Omega}| I(\vec{r_w}, \vec{\Omega}')d\Omega' \tag{2.25}$$

where $I(\vec{r_w}, \vec{\Omega})$ and $I(\vec{r_w}, \vec{\Omega}')$ are the intensities of radiation leaving and incident on the surface at a boundary location, ε_w is the surface emissivity, and $\vec{n}$ is the unit normal vector at a boundary location. The terms on the right-hand side of Equation 2.25 represent contributions to the outgoing intensity due to emission from the surface and reflection of incoming radiation.

The Equations 2.18 and 2.25 represent governing equation and its boundary condition, respectively, for radiative heat transfer. Once the intensity distribution is determined, quantities of interest such as radiative heat flux and energy source term distributions can be readily evaluated.

For the sake of clarity, the governing equations and associated initial and boundary conditions are summarized in Table 2.1

Table 2.1: Governing equations and associated initial & boundary conditions

Governing Equations	
Continuity	$\frac{\partial u}{\partial z}+\frac{\partial v}{\partial r}+\frac{v}{r}=0$
z-momentum	$\frac{\partial u}{\partial t}+u\frac{\partial u}{\partial z}+v\frac{\partial u}{\partial r}=-\frac{1}{\rho}\frac{\partial p}{\partial z}+\frac{\mu}{\rho}\left(\frac{\partial^2 u}{\partial r^2}+\frac{1}{r}\frac{\partial u}{\partial r}+\frac{\partial^2 u}{\partial z^2}\right)+\frac{1}{\rho}\left(\frac{\partial u}{\partial r}+\frac{\partial v}{\partial z}\right)\frac{\partial \mu}{\partial r}+\frac{2}{\rho}\left(\frac{\partial u}{\partial z}\right)\frac{\partial \mu}{\partial z}+g_z$
r-momentum	$\frac{\partial v}{\partial t}+u\frac{\partial v}{\partial z}+v\frac{\partial v}{\partial r}=-\frac{1}{\rho}\frac{\partial p}{\partial r}+\frac{\mu}{\rho}\left(\frac{\partial^2 v}{\partial r^2}+\frac{1}{r}\frac{\partial v}{\partial r}-\frac{v}{r^2}+\frac{\partial^2 v}{\partial z^2}\right)+\frac{2}{\rho}\left(\frac{\partial v}{\partial r}\right)\frac{\partial \mu}{\partial r}+\frac{1}{\rho}\left(\frac{\partial u}{\partial r}+\frac{\partial v}{\partial z}\right)\frac{\partial \mu}{\partial z}+g_r$
Energy	$\frac{\partial T}{\partial t}+u\frac{\partial T}{\partial z}+v\frac{\partial T}{\partial r}=\frac{k}{\rho\hat{C}_p}\left(\frac{\partial^2 T}{\partial r^2}+\frac{1}{r}\frac{\partial T}{\partial r}+\frac{\partial^2 T}{\partial z^2}\right)+\frac{1}{\rho\hat{C}_p}\left(\frac{\partial T}{\partial r}\right)\frac{\partial k}{\partial r}+\frac{1}{\rho\hat{C}_p}\left(\frac{\partial T}{\partial z}\right)\frac{\partial k}{\partial z}-\frac{\vec{\nabla}\cdot\vec{q}_R}{\rho\hat{C}_p}$
RTE	$\mu\frac{\partial I}{\partial r}-\frac{\eta}{r}\frac{\partial I}{\partial \phi}+\xi\frac{\partial I}{\partial z}=-\kappa I+\kappa I_b$
Initial & Boundary Conditions	
Initial condition	@ $t=0$ $\quad\forall r\wedge\forall z:\quad u=0,\quad v=0,\quad T=T_{ref},\quad \vec{\nabla}\cdot\vec{q}_R=0$
Boundary condition 1	@ the center $\quad\forall z\wedge\forall t:\quad \frac{\partial u}{\partial r}=0,\quad v=0,\quad \frac{\partial T}{\partial r}=0$
Boundary condition 2	@ the wall $\quad\forall z\wedge\forall t:\quad u=0,\quad v=0,\quad T=T_w$
Boundary condition 3	@ the inlet $\quad\forall r\wedge\forall t:\quad u=u_{in},\quad v=0,\quad T=T_{in}$
Boundary condition 4	@ the outlet $\quad\forall r\wedge\forall t:\quad \frac{\partial^2 u}{\partial z^2}=0,\quad \frac{\partial^2 v}{\partial z^2}=0,\quad \frac{\partial^2 T}{\partial z^2}=0$

CHAPTER 3

NUMERICAL SOLUTION TECHNIQUE

3.1 General

Numerical analysis of large-scale scientific and engineering problems has gained significant interest in the last two decades due to advancements in the processing and storage capabilities of modern computers. A number of numerical techniques and computational schemes have been proposed for the solution of PDEs governing the transport processes in these systems. Among these techniques method of lines (MOL) [63], which is a semi-discrete method, has proven to be a very accurate and efficient approach for a diverse range of applications including unsteady isothermal/non-isothermal, laminar/turbulent flows [45, 46, 48–51] and radiative heat transfer [52, 55, 56, 64]. MOL enables explicit/implicit solutions with higher-order approximations in temporal discretization and provides the flexibility in utilization of well established difference schemes for spatial discretization without additional effort in formulation. Hence, in the present study, the governing equations are solved using the MOL technique.

3.2 The Method of Lines

The method of lines consists of converting the system of partial differential equations (PDEs) into an ODE initial value problem by discretizing the spatial derivatives together with the boundary conditions via Taylor series, or weighted residual techniques and integrating the resulting ODEs using a sophisticated ODE solver which takes the burden of time discretization and chooses the time steps in such a way that maintains the accuracy and stability of the evolving solution. The most important advantage of the MOL approach is that it has not only the simplicity of the explicit methods but also the superiority (stability advantage) of the implicit ones unless

a poor numerical method for the solution of ODEs is employed. The advantages of the MOL approach are two-fold. First, it is possible to achieve higher-order approximations in the discretization of spatial derivatives without significant increases in computational complexity, and without additional difficulties with boundary conditions. Second, the use of highly efficient and reliable initial value ODE solvers means that comparable orders of accuracy can also be achieved in the time integration without using extremely small time steps.

In fact, many existing numerical algorithms for transient PDEs can be considered as MOL algorithms. The most important difference of the MOL approach from the conventional methods is that, in the MOL approach higher-order, implicit and hence stable numerical algorithms for time integration are used. For the numerical solution of the same PDE system, the MOL approach and the conventional methods, in which a lower-order either explicit or implicit time-integration methods are used, have the same system of ODEs as a result of spatial discretization. Therefore, stability of the ODE problem should be satisfied not only for the MOL approach but also for the conventional methods. However, it should be noted that satisfaction of the stability of the ODE system as a result of spatial discretization does not necessarily mean that the final solution as a result of time-integration will also be stable. So, in order to have absolutely stable and accurate solutions, the first condition is to satisfy the ODE problem stability, and the second one is to use sophisticated (higher-order and implicit) time-integration methods. In the present study, the first is provided by utilizing a second-order TVD scheme based on Lagrange interpolation polynomial [65] for the convective terms and a fourth-order centered scheme based on Lagrange interpolation polynomial for the diffusive terms in the CFD code and a two-point upwind differencing scheme in the radiation code. Second, time integration is achieved by using higher-order and stable schemes embedded in quality ODE solvers; LSODES and RKF45 in CFD and radiation codes, respectively.

3.3 Spatial Discretization of the PDEs Governing the Fluid Dynamics

The discretization of spatial terms appearing in the governing equations requires particular consideration. Inappropriate discretization of these terms leads to an unstable ODE problem for both conventional and MOL algorithms.

The nature of convection process necessitates the use of upwind methods in which the information for each variable is obtained by looking in the direction from which this information should be coming. In order to met this requirement, in the present study an adaptive spatial discretization scheme which decides whether to use upwind or downwind discretization in a zone-of-dependence manner is utilized for the approximation of convective terms [46]. The adaptive stencil scheme is accommodated into the code as follows. The code checks the signs of the coefficients of the convective derivatives ($\frac{\partial u}{\partial z}$, $\frac{\partial u}{\partial r}$, $\frac{\partial T}{\partial z}$, $\frac{\partial T}{\partial r}$) and decides whether an upwind or downwind discretization scheme is to be used. If the coefficient is positive, discretization of convective derivatives are carried out by an upwind scheme as the information is gathered from the upstream direction. If the coefficient is negative, a downwind scheme is used as the zone-of-dependence is downstream of the point under consideration. Implementation of this procedure into the computer code is performed by writing convective derivatives as follows

$$\left.\frac{\partial \varsigma}{\partial \bar{x}}\right|_i = \frac{C}{2}\left[(1-\varepsilon_C)\left.\frac{\partial \varsigma}{\partial \bar{x}}\right|_d + (1+\varepsilon_C)\left.\frac{\partial \varsigma}{\partial \bar{x}}\right|_u\right] \tag{3.1}$$

where ς is the pseudo one-dimensional dependent variable at any point along the $\bar{x}$ direction at any time. C denotes the coefficients of the convective derivatives. Subscripts d and u denote downwind and upwind stencils, respectively, and

$$\varepsilon_C = sign(C) = \frac{C}{|C|}. \tag{3.2}$$

In the present study, the convective terms near and at the boundaries were evaluated by the first-order approximation.

Diffusive terms appearing in the governing equations include second-order derivatives of the dependent variables. Since they correspond to diffusive effects, they are

always centrally discretized [66]. One approach in approximating a second-order derivative is the stagewise differentiation of the first-order derivatives [63]. In the present study this approach is followed for evaluation of diffusion terms by stagewise differentiation of first-order centered derivatives obtained from fourth-order centered scheme based on Lagrange interpolation polynomial. Hence, more accurate solutions can be obtained by high-order discretization of diffusive terms.

3.4 Treatment of Pressure

The computation of pressure is the most difficult and time-consuming part of the overall solution of the Navier-Stokes equations and involves the iterative procedure between the velocity and pressure fields through the solution of a Poisson-type equation for pressure to satisfy divergence-free condition for confined incompressible flows. Therefore, in this study, a noniterative procedure for the calculation of pressure suggested by [67], and [68] and applied by [47] is used. This procedure is based on the fact that in the numerical solution of the Navier-Stokes equations for internal flows, the streamwise pressure gradient must be known in such a way that the mass conservation at each cross-section is satisfied. In order to accomplish this, the static pressure $p(r,z,t)$ in the momentum equations is split into two parts

$$p(r,z,t) = \hat{p}(z,t) + \tilde{p}(r,z,t) \tag{3.3}$$

as suggested in [67] and [68].

As can be seen from Equation (3.3), $\hat{p}$ is independent of r-direction. Hence, the derivative of Equation (3.3) with respect to z- and r-directions yields

$$\frac{\partial p}{\partial z} = \frac{\partial \hat{p}}{\partial z} + \frac{\partial \tilde{p}}{\partial z}, \tag{3.4}$$

and

$$\frac{\partial p}{\partial r} = \frac{\partial \tilde{p}}{\partial r}. \tag{3.5}$$

The physical assumption in this decoupling procedure is that $\frac{\partial \tilde{p}}{\partial z}$ is very small compared with $\frac{\partial \hat{p}}{\partial z}$. Therefore, when the pressure field is split into two in this manner, the momentum equations can be written as follows.

r-momentum;

$$\begin{aligned}\frac{\partial v}{\partial t}+u\frac{\partial v}{\partial z}+v\frac{\partial v}{\partial r} = & -\frac{1}{\rho}\frac{\partial \tilde{p}}{\partial r}+\frac{\mu}{\rho}\left(\frac{\partial^2 v}{\partial r^2}+\frac{1}{r}\frac{\partial v}{\partial r}-\frac{v}{r^2}+\frac{\partial^2 v}{\partial z^2}\right)\\ & +\frac{2}{\rho}\left(\frac{\partial v}{\partial r}\right)\frac{\partial \mu}{\partial r}+\frac{1}{\rho}\left(\frac{\partial u}{\partial r}+\frac{\partial v}{\partial z}\right)\frac{\partial \mu}{\partial z}+g_r, \end{aligned} \tag{3.6}$$

z-momentum;

$$\begin{aligned}\frac{\partial u}{\partial t}+u\frac{\partial u}{\partial z}+v\frac{\partial u}{\partial r} = & -\frac{1}{\rho}\frac{\partial \hat{p}}{\partial z}+\frac{\mu}{\rho}\left(\frac{\partial^2 u}{\partial r^2}+\frac{1}{r}\frac{\partial u}{\partial r}+\frac{\partial^2 u}{\partial z^2}\right)\\ & +\frac{1}{\rho}\left(\frac{\partial u}{\partial r}+\frac{\partial v}{\partial z}\right)\frac{\partial \mu}{\partial r}+\frac{2}{\rho}\left(\frac{\partial u}{\partial z}\right)\frac{\partial \mu}{\partial z}+g_z. \end{aligned} \tag{3.7}$$

The pressure gradient in Equation (3.7), $\frac{\partial \hat{p}}{\partial z}$, can be determined with the aid of global mass flow constraint combined with the discretized form of the z-momentum equation. For this purpose the temporal derivative in Equation (3.7) is discretized, and the following equation is obtained.

$$\begin{aligned}\frac{u_{i,j}^{n+1}-u_{i,j}^{n}}{\Delta t} = & -\frac{1}{\rho}\left(\frac{\partial \hat{p}}{\partial z}\right)_j^n-\left[u_{i,j}^{n}\left(\frac{\partial u}{\partial z}\right)_{i,j}^{n}+v_{i,j}^{n}\left(\frac{\partial u}{\partial r}\right)_{i,j}^{n}\right]\\ & +\frac{\mu}{\rho}\left[\left(\frac{\partial^2 u}{\partial r^2}\right)_{i,j}^{n}+\frac{1}{r}\left(\frac{\partial u}{\partial r}\right)_{i,j}^{n}+\left(\frac{\partial^2 u}{\partial z^2}\right)_{i,j}^{n}\right]\\ & +\frac{1}{\rho}\left[\left(\frac{\partial u}{\partial r}\right)_{i,j}^{n}+\left(\frac{\partial v}{\partial z}\right)_{i,j}^{n}\right]\left(\frac{\partial \mu}{\partial r}\right)_{i,j}^{n}\\ & +\frac{2}{\rho}\left(\frac{\partial u}{\partial z}\right)_{i,j}^{n}\left(\frac{\partial \mu}{\partial z}\right)_{i,j}^{n}+g_z. \end{aligned} \tag{3.8}$$

Rearranging Equation (3.8) yields

$$u_{i,j}^{n+1}=\Phi_{i,j}^{n}+\left(\frac{\partial \hat{p}}{\partial z}\right)_j^n\Psi^n, \tag{3.9}$$

where

$$\begin{aligned}\Phi_{i,j}^{n} = u_{i,j}^{n} & -\Delta t\left\{u_{i,j}^{n}\left(\frac{\partial u}{\partial z}\right)_{i,j}^{n}+v_{i,j}^{n}\left(\frac{\partial u}{\partial r}\right)_{i,j}^{n}\right.\\ & -\frac{\mu}{\rho}\left[\left(\frac{\partial^2 u}{\partial r^2}\right)_{i,j}^{n}+\frac{1}{r}\left(\frac{\partial u}{\partial r}\right)_{i,j}^{n}+\left(\frac{\partial^2 u}{\partial z^2}\right)_{i,j}^{n}\right]\\ & -\frac{1}{\rho}\left[\left(\frac{\partial u}{\partial r}\right)_{i,j}^{n}+\left(\frac{\partial v}{\partial z}\right)_{i,j}^{n}\right]\left(\frac{\partial \mu}{\partial r}\right)_{i,j}^{n}\\ & \left.-\frac{2}{\rho}\left(\frac{\partial u}{\partial z}\right)_{i,j}^{n}\left(\frac{\partial \mu}{\partial z}\right)_{i,j}^{n}-g_z\right\}, \end{aligned} \tag{3.10}$$

and

$$\Psi^n = -\frac{\Delta t}{\rho^n}. \tag{3.11}$$

where n and $n+1$ represent the present and advanced time levels. Equation (3.9) is then multiplied by the density ρ^{n+1} and the resulting equation is subsequently integrated numerically over the cross-sectional area perpendicular to the streamwise direction. This yields

$$\int_A \rho^{n+1} u_{i,j}^{n+1} dA = \dot{m} = \int_A \rho^{n+1} \Phi_{i,j}^n dA + \left(\frac{\partial \hat{p}}{\partial z}\right)_j^n \int_A \rho^{n+1} \Psi_{i,j}^n dA, \tag{3.12}$$

where

$$dA = r dr d\theta, \tag{3.13}$$

in cylindrical coordinates.

Since the mass flow is prespecified by the problem inlet boundary condition, the pressure gradient $\frac{\partial \hat{p}}{\partial z}$ can be computed from the following expression obtained by rearranging Equation (3.12)

$$\left(\frac{\partial \hat{p}}{\partial z}\right)_j^n = \frac{2\pi\rho \int_0^R \Phi_{i,j}^n r dr - \dot{m}}{\pi R^2 \Delta t}. \tag{3.14}$$

Here, $\dot{m}$ is mass flow rate prescribed as inlet condition and R is the radius of the burner.

3.5 Computation of Radial Velocity Component

In the present study, in order not to bring an extra burden to the ODE solver, the r-component velocity $v(r,z,t)$ is determined with the direct utilization of the continuity equation. For this purpose the continuity equation is discretized as

$$\frac{1}{r_i}\left(\frac{r_{i+1} v_{i+1,j}^n - r_i v_{i,j}^n}{\Delta r_i^+}\right) = -\left(\frac{\partial u}{\partial z}\right)_{i,j}^n, \tag{3.15}$$

and Equation 3.15 is rearranged to yield

$$v_{i+1,j}^n = \frac{r_i}{r_{i+1}}\left[v_{i,j}^n - \Delta r_i^+ \left(\frac{\partial u}{\partial z}\right)_{i,j}^n\right], \tag{3.16}$$

where

$$i = 1, \ldots, NR-2, \qquad j = 2, \ldots, NZ, \qquad \Delta r_i^+ = r_{i+1} - r_i. \tag{3.17}$$

Hence, by this formulation, not only the r-component velocity is computed without bringing an extra burden to the ODE solver used for time integration, but also the divergence-free condition for incompressible flows is satisfied automatically.

3.6 Time Integration

As mentioned earlier, MOL consists of two stages; (1) spatial discretization of PDEs, (2) integration of the resultant system of ODEs. In this section, the second stage of the MOL solution which is the time integration of the governing equations, will be described.

Substitution of the approximations of spatial derivatives into the governing equations yields the following set of ODEs in time;

$$\frac{d\bar{\phi}}{dt} = f\left(\bar{\phi}\right), \qquad \bar{\phi} = \left(\phi_1, \phi_2, \ldots, \phi_{NEQN}\right), \tag{3.18}$$

where $NEQN$ denotes the number of equations to be solved and $\bar{\phi}$ is a one-dimensional dummy vector containing the dependent variables ϕ. The resulting system with suitable initial and boundary conditions is integrated by any of the ODE integration methods, e.g, explicit Euler's method, Runge-Kutta method, Backward Differentiation Formula (BDF), etc.

As mentioned before, the most important feature of the MOL approach is that it has not only the simplicity of the explicit methods but also the superiority of the implicit ones as the higher-order implicit time integration methods are employed in the solution of the resulting stiff system of ODEs. The stiff ODE concept is well established and various efficient and reliable stiff ODE solvers, having the advantage of the use of variable time steps and order of the method, are available in the open literature [63, 69–71]. However, it is very important to select a suitable one considering type and dimension of the physical system, desired level of accuracy and execution time. In the present study, a higher-order and stable schemes embedded in quality ODE solver; LSODES was used.

3.7 Computation of Radiative Energy Source Term

As mentioned earlier, in flow applications where combined convective and radiative heat transfer take place, the radiative energy source term (divergence of the radiative heat flux) have to be implemented in the classical energy conservation equation of the CFD calculations. In order to calculate the radiative energy source term, first RTE should be solved. MOL solution of Discrete Ordinates Method (DOM) is a promising method for the solution of the RTE due to its accuracy and compatible formulation with that for governing flow equations. In the following sections DOM and its MOL solution will be explained.

3.7.1 Discrete Ordinates Method

DOM is based on representation of continuous angular domain by a discrete set of ordinates with appropriate angular weights, spanning the total solid angle of 4π steradians. The discrete ordinates representation of the RTE for an absorbing-emitting gray medium in axisymmetric cylindrical coordinate system takes the following form

$$\frac{\mu_m}{r}\frac{\partial(rI^m)}{\partial r} - \frac{1}{r}\frac{\partial(\eta_m I^m)}{\partial \phi} + \xi_m \frac{\partial I^m}{\partial z} = -\kappa I^m + \kappa I_b \tag{3.19}$$

where $I^m[\equiv I(r,z;\theta,\phi)]$ is the total radiation intensity at position (r,z) in the discrete direction Ω_m. The terms on the left hand-side represents the gradient of intensity in curvilinear coordinates, and the two terms on the right hand-side stand for the changes in intensity due to absorption and emission, respectively.

The angular derivative term, which makes the solution of DOM complicated, is discretized by introducing an angular redistribution term $\gamma_{m,\ell\pm1/2}$, proposed by Carlson and Lathrop [72]. After discretization, the angular derivative term takes the following form

$$\left[\frac{\partial(\eta_m I^m)}{\partial \phi}\right]_{\Omega_m=\Omega_{m,\ell}} = \left(\frac{\gamma_{m,\ell+1/2} I^{m,\ell+1/2} - \gamma_{m,\ell-1/2} I^{m,\ell-1/2}}{w_{m,\ell}}\right) \tag{3.20}$$

where $I^{m,\ell+1/2}$ and $I^{m,\ell-1/2}$ are radiation intensities in directions $m,\ell+1/2$ and $m,\ell-1/2$ which define the edges of angular range of $w_{m,\ell}$. Mathematically, these

terms and the angular redistribution term can be expressed as

$$I^{m,\ell+1/2} = \frac{I^{m,\ell} + I^{m,\ell+1}}{2}, \tag{3.21}$$

$$I^{m,\ell-1/2} = \frac{I^{m,\ell-1} + I^{m,\ell}}{2}, \tag{3.22}$$

and

$$\gamma_{m,\ell+1/2} = \gamma_{m,\ell-1/2} + \mu_{m,\ell} w_{m,\ell} \qquad \ell = 1,2...L \tag{3.23}$$

where, L is the maximum value of ℓ for a particular m. Further details of angular redistribution terms and estimation of the angular derivative can be found from [55, 73]. Equations 3.19 and 3.20, and the recurrence relations (Equations 3.21, 3.22, and 3.23) yield discrete ordinates equations for axisymmetric cylindrical geometry. The final form of discrete ordinates equation for axisymmetric cylindrical geometry takes the following form

$$\frac{\mu_{m,\ell}}{r}\frac{\partial(rI^{m,\ell})}{\partial r} - \frac{1}{r}\frac{(\gamma_{m,\ell+1/2}I^{m,\ell+1/2} - \gamma_{m,\ell-1/2}I^{m,\ell-1/2})}{w_{m,\ell}} + \xi_{m,\ell}\frac{\partial I^{m,\ell}}{\partial z} = -\kappa I^{m,\ell} + \kappa I_b \tag{3.24}$$

The quadrature ordinates and weights for axisymmetric cylindrical geometry of S_N approximations are listed in Appendix A. Boundary conditions required for the solution of the Equation 3.24 on the surface of the enclosure take the following forms for diffusely emitting-remitting surfaces at z=0;

$$I^{m,\ell} = \varepsilon_w I_b(\vec{r_w}) + \frac{(1-\varepsilon_w)}{\pi}\sum_{m',\ell'} w_{m',\ell'}\left|\xi_{m',\ell'}\right| I^{m',\ell'} \qquad \xi_{m,\ell} > 0 \tag{3.25}$$

at z=L;

$$I^{m,\ell} = \varepsilon_w I_b(\vec{r_w}) + \frac{(1-\varepsilon_w)}{\pi}\sum_{m',\ell'} w_{m',\ell'}\xi_{m',\ell'} I^{m',\ell'} \qquad \xi_{m,\ell} < 0 \tag{3.26}$$

at r=R;

$$I^{m,\ell} = \varepsilon_w I_b(\vec{r_w}) + \frac{(1-\varepsilon_w)}{\pi}\sum_{m',\ell'} w_{m',\ell'}\mu_{m',\ell'} I^{m',\ell'} \qquad \mu_{m,\ell} < 0 \tag{3.27}$$

at r=0;

$$I^{m,\ell} = I^{m',\ell'} \qquad \mu_{m,\ell} > 0 \tag{3.28}$$

In Equations 3.25- 3.28, the values m,ℓ and m',ℓ' denote outgoing and incoming directions respectively. In the present study, the wall surface, and inlet and outlet imaginary surfaces were assumed to be radiatively black.

3.7.2 Method of Lines Solution of Discrete Ordinates Methods

The solution of discrete ordinates equations with MOL is carried out by adoption of the false-transients approach which involves incorporation of a pseudo-time derivative of intensity into the discrete ordinates equations [74]. Adoption of the false-transient approach to Equation 3.24 yields

$$\begin{aligned} k_{t^*}\frac{\partial I^{m,\ell}}{\partial t} = & - \frac{\mu_{m,\ell}}{r}\frac{\partial (rI^{m,\ell})}{\partial r} + \frac{1}{r}\frac{(\gamma_{m,\ell+1/2}I^{m,\ell+1/2} - \gamma_{m,\ell-1/2}I^{m,\ell-1/2})}{w_{m,\ell}} - \xi_{m,\ell}\frac{\partial I^{m,\ell}}{\partial z} \\ & - \kappa I^{m,\ell} + \kappa I_b \end{aligned} \tag{3.29}$$

where t^* is the pseudo-time variable and k_{t^*} is a time constant with dimension $[(m/s)^{-1}]$ which is introduced to maintain dimensional consistence in the equation and it is taken as unity.

The system of PDEs with initial and boundary-value independent variables is then transformed into an ODE initial value problem by using MOL approach [55]. The transformation is carried out by representing the spatial derivatives with the algebraic finite-difference approximations. Thus, the first stage of MOL solution; discretization of all the spatial terms appearing in the RTE is accomplished. The details of angular and spatial discretization can be found from [55].

The second stage of MOL solution which is time integration of the resultant system of ODEs is carried out in a similar fashion as in the CFD code. Starting from an initial condition for radiation intensities in all directions, the system of ODEs is integrated until steady state by using a powerful ODE solver. Any initial condition can be chosen to start the integration, as its effect on the steady state solution decays

to insignificance. To stop the integration at steady state, a convergence criterion is checked for all intensities.

Once the intensity distribution is determined by solving Equation 3.29 together with its boundary conditions, the radiative energy source term can be obtained from the following equation

$$\vec{\nabla} \cdot \vec{q}_R = \kappa \left(4\pi I_b - \sum_m \sum_\ell w_{m,\ell} I^{m,\ell} \right) \tag{3.30}$$

In the present study, the spatial terms of RTE are discretized by using two-point upwind differencing scheme. The S_4 order of approximation was found to be optimum by succesive refinement studies [75]. RKF45 (Runge-Kutta-Fehlberg integration) subroutine [49], which is an adaptive, fourth order accurate ODE solver, was utilized for time integration.

3.8 Computation of Thermophysical and Radiative Properties

In strongly non–isothermal systems, evaluation of temperature dependent thermophysical properties plays an important role in the numerical solution of fluid-flow equations. In the present study, transport properties, namely, viscosity and thermal conductivity, were calculated using the TRANSPORT package by Kee *et al.* [76]. Thermodynamic properties, namely, the density and specific heat, are evaluated using CHEMKIN-III [77] and its database. The temperature and concentration-dependent absorption coefficients for the gray gas were calculated using Leckner's correlation [78].

3.9 Description of the Coupling Procedure and Mode of Operation of the Sequential Code

In this study, a numerical methodology developed by Selçuk *et al.* [44] is utilized for the solution of time-dependent Navier-Stokes equations in conjunction with the RTE in two-dimensional axisymmetric, cylindrical geometry. The proposed methodology has the following novel features: (1) CFD code is based on DNS approach which is the most reliable way to analyze turbulent flows, (2) the solution methods for the CFD

code and the radiation code are compatible as they are based on the same approach, namely MOL.

Coupling strategy between the CFD and radiation codes is mainly based on periodic transfer of temperature field solved by the flow code to the radiation code which in turn provides the source term field to be inserted in the energy equation. The schematic representation of the coupling procedure is illustrated in Figure 3.1. A variable mesh size in both *r* and *z* directions was used which are clustered to the wall in *r* and to the inlet in *z* directions, respectively. Since using identical grid resolutions for both fluid flow and radiation transport would be very expensive, two different grid resolutions are established; a fine mesh which would meet the DNS requirement for fluid flow and a coarse one enabling economic computation of radiative energy source term (See Figure 3.2).

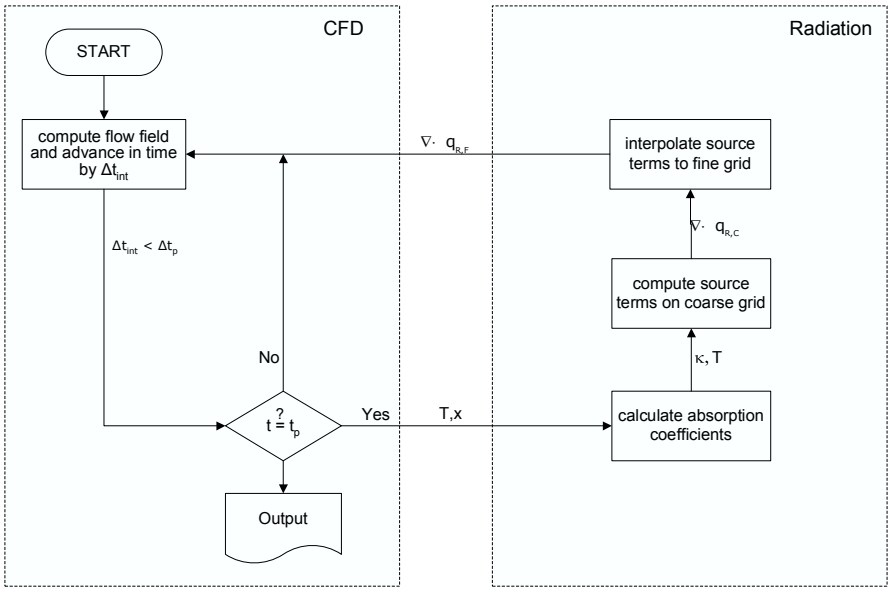

Figure 3.1: Coupling Procedure.

Figure 3.3 shows the organization of the sequential coupled code in which all the subroutines are executed sequentially. The whole procedure can be summarized as follows.

All dependent variables are known *a priori* at the beginning of each cycle, either as a result of the previous cycle or from the prescribed initial conditions. First, in the CFD

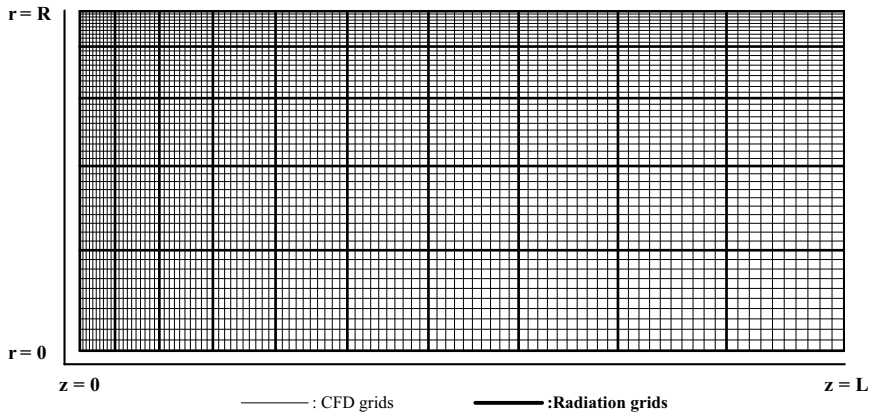

Figure 3.2: Representative grid structure.

code, transport and thermodynamic properties of the medium are calculated using the known temperature field. Then the spatial derivatives appearing in the governing flow equations are evaluated using values of the present cycle, and the radial component of velocity is determined by the direct utilization of the continuity equation, so that divergence-free condition is ensured automatically. Then the corresponding pressure gradients along the axial direction are calculated to ensure that the mass flow is conserved. Once these calculations have been made, the time derivative vector is calculated over the spatial domain, than it is sent to the ODE solver to compute the dependent variables at the advanced time level. This completes the progression of the solution to the end of the new cycle having the new values of the velocity and temperature fields. This procedure is repeated until ODE solver reaches the user defined time step t_p and when the t_p is reached the new temperatures at the overlapping grid points of the coarse and fine meshes are transferred to the radiation code which in turn provides radiative energy source term at the same grid points for the CFD code. Source terms on the coarse mesh are redistributed to the fine mesh of CFD code via 2-D interpolation. With these source terms, CFD code continues marching in time. Upon the next call, the radiation code commences with the final intensities from the previous call to obtain faster convergence. This cyclic procedure is repeated until steady-state is reached. It is worth noting here that Δt_p is not necessarily equal to the time step Δt_{int} chosen by the ODE solver. The ODE solver chooses much smaller internal time steps Δt_{int} than Δt_p. Another role attributed to

Δt_p, other than being the time interval at which the code produces output, is that the same source term field for the solution of fluid-flow equations is used throughout the interval Δt_p. This is an approach called loosely coupled method which significantly reduces the CPU time of the code without any comprise from accuracy.

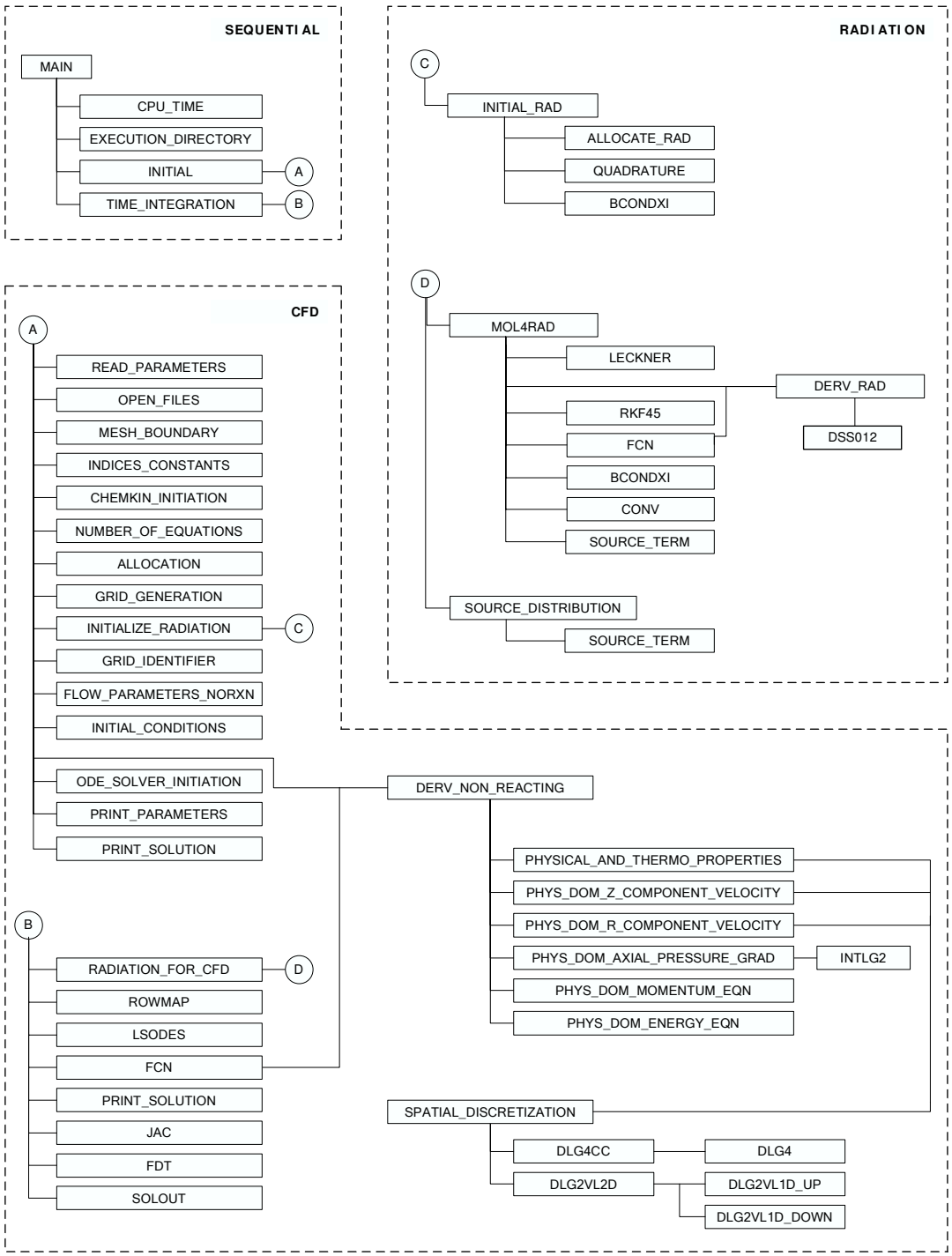

Figure 3.3: Organization of sequential coupled code.

CHAPTER 4

PARALLEL IMPLEMENTATION OF THE COUPLED CODE

4.1 General

In this chapter, parallel implementation of the sequential coupled code will be explained by basic principles of parallelization.

4.2 Parallelization

Parallelization is a strategy for performing large and complex tasks with extensive execution time and memory requirements. Such tasks can either be performed sequentially, one step following another, or can be decomposed into smaller tasks to be performed simultaneously, i.e. in parallel. Parallelization is carried out by

- Decomposing the task into smaller tasks
- Assigning the smaller tasks to multiple processors to work on simultaneously
- Communication among processors

In spite of the advances in the processor technology, the need to dissipate large amount of energy in a small volume and the finite speed of light limit the maximum speed of a single processor. Present day computers are reaching this limit, which is about 10 billions of instructions per second. This prevents the serial computers to be able to perform the computation requirement in many of the scientific and engineering problems [79–81]

The aforementioned limitation makes parallel computing an alternative over serial one in many different areas which require handling of large amounts of data such as

image processing, database applications, climate modelling, combustion systems and turbulence etc.

4.3 Parallelization Strategy

One of the first steps in conceiving a parallel algorithm is decomposing a large problem into smaller discrete "*chunks*" of work that can be distributed to multiple tasks, i.e., units of computation. This can be achieved in two ways; functional decomposition and domain decomposition. In functional decomposition, the problem is partitioned according to the work that must be done. Each task then performes a portion of the overall work on different processors simultaneously. These tasks may be considered as subroutines of the main program which do not require other's outputs as the inputs, hence, can be executed at the same time. In Figure 4.1 the implementation of functional decomposition method is illustrated. Each block defined by a letter represents a task. At the top of the figure the logical sequence of the tasks is given, and at the bottom the way in which they are executed in the serial and parallel cases are represented.

In domain decomposition, the main domain is divided into smaller domains, which are called sub-domains. Each sub-domain can be considered as a domain. Calculations are carried out independently in each sub-domain and their solutions are combined to obtain solution for the main domain. In this technique, the neighbor sub-domains require information exchange as they share the same boundary conditions in between them. The schematic representation of the technique is shown in Figure 4.2.

In a recent study, carried out by Erşahin *et al.* [50] a MOL based DNS code has been parallelized using domain decomposition technique by means of overlapping boundary at the intergrid regions to provide the information exchange between the sub-domains. Five point discretization scheme which necessitates at least three points exchange among the neighbor sub-domains was utilized. In this thesis study parallel implementation of the sequential coupled code is performed by utilizing the methodology proposed by Erşahin *et al.* [50]. In this methodology each sub-domain is assigned with a *type* which is determined according to the position of that sub-domain

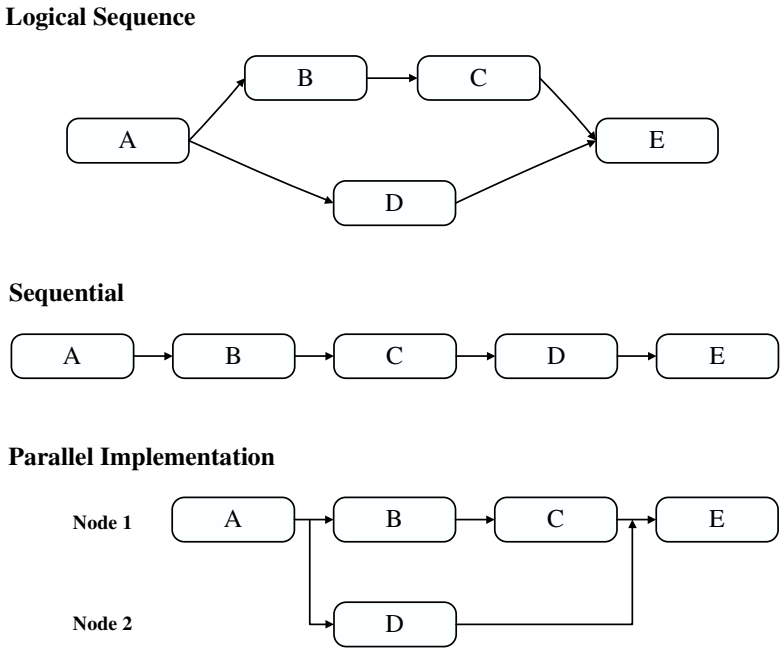

Figure 4.1: Functional decomposition.

relative to the other sub-domains. In other words, the first sub-domain near to inlet is assigned as *type*-1, which includes an inlet boundary condition and an imaginary boundary condition; the last sub-domain near exit is assigned as *type*-3, which includes an imaginary boundary condition and an outlet boundary condition; and the intermediate sub-domains are assigned as *type*-2, which include two imaginary

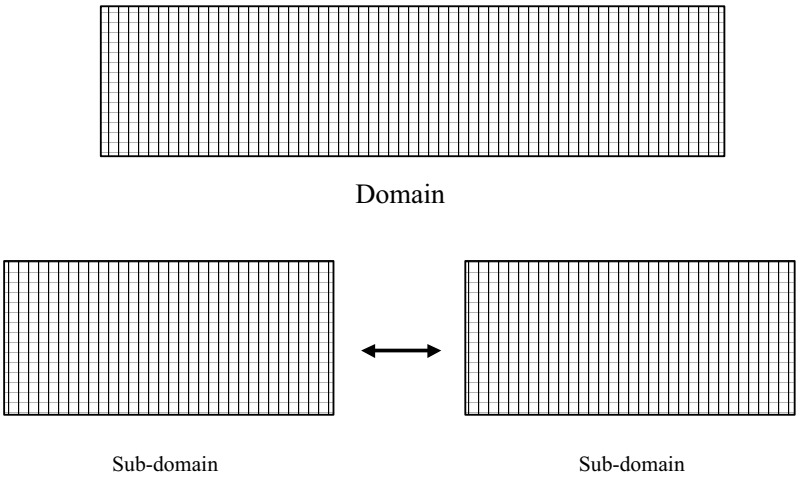

Figure 4.2: Domain decomposition.

boundary conditions.

The information exchange between the sub-domains occurs at the adjacent imaginary boundaries. For example, as depicted in Figure 4.3, the information exchange between the sub-domains of *type*-1 and *type*-2 is provided through the transfer of final three grid lines, i.e., *nz*-5, *nz*-4, *nz*-3 from sub-domain of *type*-1 to sub-domain of *type*-2 which, in turn, sends the first three grid lines, i.e., 4, 5, 6. This protocol is valid for all the information exchange between the sub-domains, regardless of their *types*.

4.4 Parallel Implementation of the Coupled Code

As mentioned earlier, parallel implementation of the coupled code will be carried out by using domain decomposition technique with overlapping grids at the imaginary boundaries. At this point it is believed that the concept of information exchange between the sub-domains should be explained in more detail since it constitutes the core of domain decomposition technique. The variables to be exchanged are axial velocity (u), temperature (T) for the CFD code and intensity (I) for the radiation code. 5-point discretization scheme based on biased-upwind or biased-downwind stencils used in the CFD code and 2-point upwind discretization scheme used in the radiation code, necessitates, at least three points for the CFD code (See Figure 4.3) and one point for the radiation code (See Figure 4.4) to be exchanged between the neighboring sub-domains at user defined time steps. When Figure 4.4 is closely examined, it will be seen that instead of transferring the intensities at all directions, only the direction which will affect neighboring domain is transferred. For instance, in order for the intensity field in the domain of *type-1* (left domain) to feel the effect of the intensity field in the domain of *type-2* (right domain), the intensities at the boundaries with negative z direction should be transferred from right to left and vice-versa.

4.5 Message Passing

Message passing provides the information exchange between the processors. There are some software tools that provide this exchange; Parallel Virtual Machine (PVM)

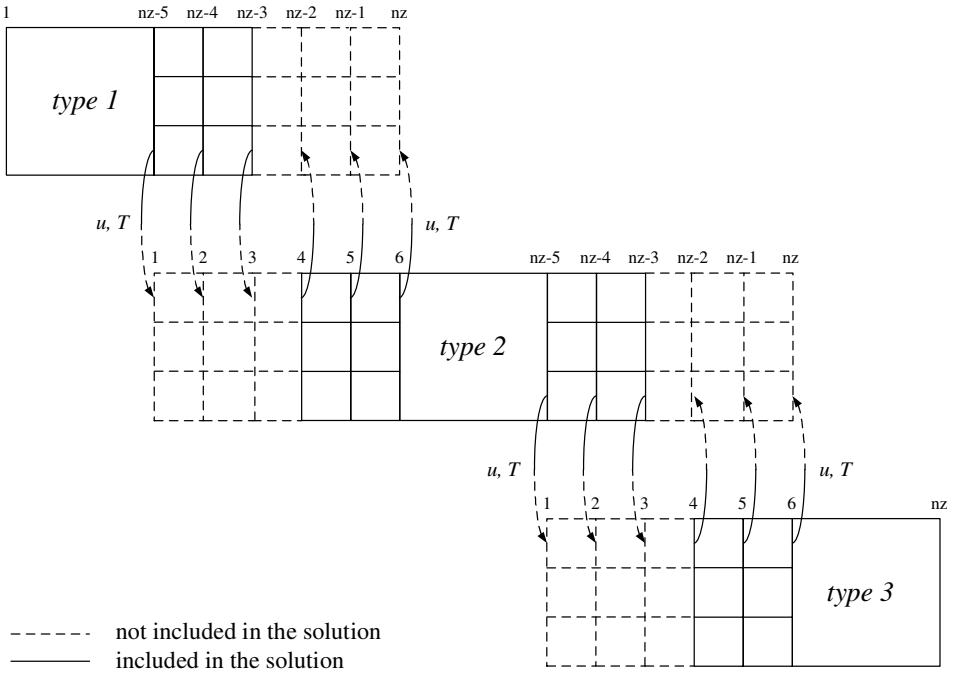

Figure 4.3: Three point exchange with six points overlap paradigm for the CFD code.

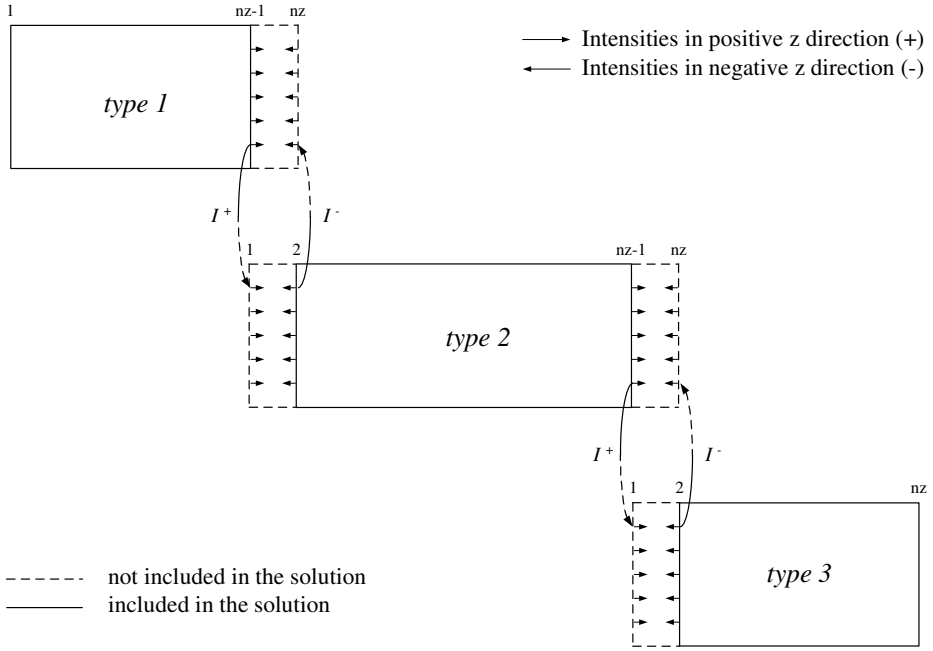

Figure 4.4: One point intensity exchange with two points overlap paradigm for the radiation code.

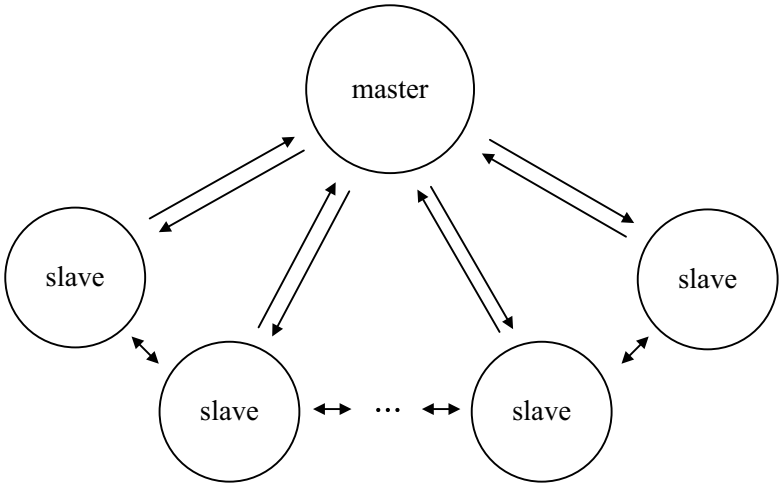

Figure 4.5: Master-slave paradigm.

and Message Passing Interface (MPI) are two of them. Both MPI and PVM have FORTRAN and C libraries, which provide subroutines for adding hosts, starting-up and killing processes, receiving and sending information between the hosts. These subroutines are called inside the program for communication among the processors. In this study PVM is used as the message passing software because of its compatibility in different computer architectures, our experience in PVM and its freeware distribution.

In a message-passing algorithm there are two processes: master process and slave processes. Master process starts necessary number of slave programs, coordinates their jobs and communications between slaves and itself (Figure 4.5). The slave processes are the parts where main task is performed. As many slave processes as required may be started by spawning them in the master process. A task is assigned to each slave by the master process and the slaves execute their own task with their own data by making required communications during the runs. At some certain time steps they send their intermediate solutions to master program and the master can obtain the full solution by combining the intermediate solutions coming from all slaves.

4.6 Performance Criteria

The purpose of parallelization is to decrease execution time for the solution of a problem. The performance of a parallel algorithm is evaluated with the following

parameters:

- Speed-up
- Efficiency
- Cost

Speed-up is the measure of relative performance as a function of number of processors employed. Speed-up is shown by S and is defined as,

$$S = \frac{t_{sp}}{t_{mp}}$$

where, t_{sp} and t_{mp} represent the execution times, using a single processor and p processors, respectively.

One other parameter for evaluating performance is the efficiency. It is abbreviated by E and defined as,

$$E = \frac{S}{p}$$

where S is the speed-up and p is the number of processors employed. Efficiency is a measure of the fraction of the time that processors are being used for computation. Hence higher the efficiency, larger the ratio of computation to communication time is.

Another parameter for performance evaluation is cost. Cost is simply total execution time.

$$Cost = (Execution\,Time) \times (Number\,of\,Processors)$$

For high performance, the speed-up and efficiency should be as high as possible whereas for an economical solution cost should be low.

4.7 Structure and Operation of the Parallel Code

Figure 4.6 summarizes the organization of parallel coupled code. The algorithm is based on the master-slave paradigm, where the master process generates the grid structure, sets the initial and physical boundary conditions, decomposes the domain

into sub-domains having the same number of grid points, sets the (*type*) of each sub-domain and sends the related information to the slave processes. The slave processes with the instructions supplied perform the calculations for the sub-domains assigned to them according to the types set by the master process, advance in time and exchange necessary information between each other at user defined time steps t_p and send transient results to the master process for the development of the transient solution until steady state is reached.

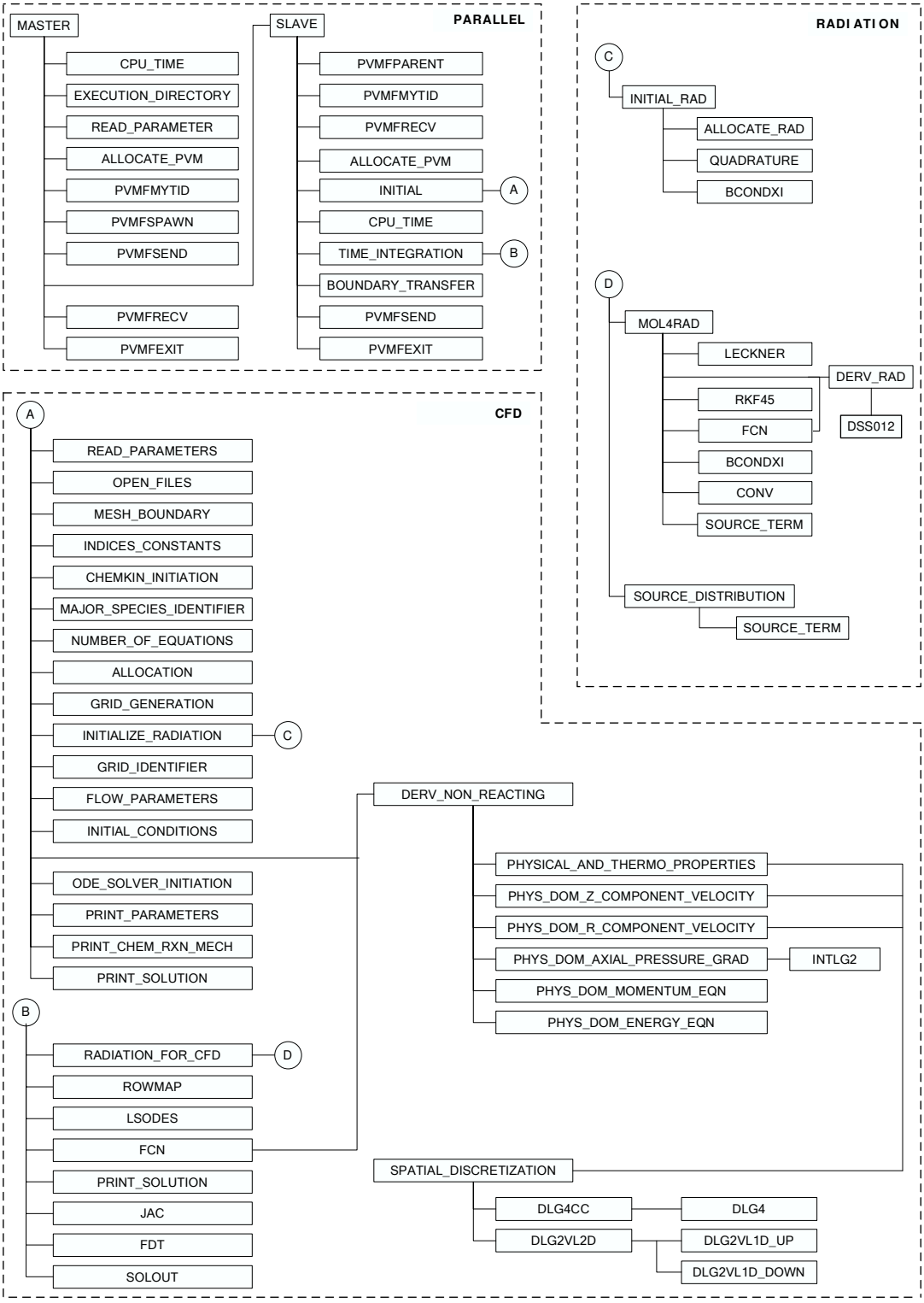

Figure 4.6: Organization of parallel coupled code.

CHAPTER 5

RESULTS AND DISCUSSION

5.1 General

The coupled code was applied to the prediction of heat transfer and flow charateristics in thermally radiating laminar/turbulent flow of gray gases through axisymmetric cylindrical geometries, and validated by comparing its predictions with the numerical solutions available in the literature. The code was then applied to the prediction of transient turbulent radiating flow of carbon dioxide through a cylindrical pipe with an abrupt change in wall temperature. The effects of Reynolds number and upstream propagation of radiation on the temperature and velocity fields were examined in detail. In what follows, the respective test cases will be described and the results obtained will be discussed.

5.2 Test Case I: Validation of the Coupled Code for Thermally Radiating Laminar Pipe Flow

In order to assess the predictive accuracy of the coupled code, it was first applied to the prediction of thermally radiating laminar gas flow through a circular pipe for which numerical solution had been reported previously in the literature (Baek *et al.* [31]). The temperature predictions of the code were benchmarked against the numerical solution of Baek *et al.* [31].

The system under consideration consists of an absorbing emitting gray gas flowing steadily through a cylindrical black-walled pipe of length L and diameter D as depicted in Figure 5.1. The aspect ratio (D/L) is 0.1. The fluid enters the pipe with a uniform temperature T_{in} and a fully developed laminar velocity profile. The flow inside the pipe is hydrodynamically developed. The wall of the pipe is at constant

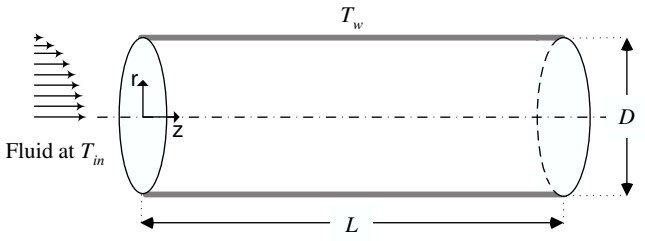

Figure 5.1: Schematic representation of the system.

temperature, T_w, and the inlet to wall temperature ratio (T_{in}/T_w) is =0.6. The inlet and outlet of the pipe are assumed to be radiatively black imaginary surfaces at fluid temperature. The Péclet number ($= Re.Pr$) is equal to 200, and the optical thickness of the medium, $\tau_D (= \kappa D)$, is 0.5. The medium is incompressible with constant thermophysical properties at atmospheric pressure. The imposed initial and boundary conditions are listed in Table 5.1.

Table 5.1: Initial & boundary conditions.

I.C.	@ $t = 0$	$\forall r \wedge \forall z:$	$u = 0,$	$v = 0,$	$T = T_{ref}$	$\vec{\nabla} \cdot \vec{q}_R = 0$
B.C. 1	@ the center	$\forall z \wedge \forall t:$	$\frac{\partial u}{\partial r} = 0,$	$v = 0,$	$\frac{\partial T}{\partial r} = 0$	
B.C. 2	@ the wall	$\forall z \wedge \forall t:$	$u = 0,$	$v = 0,$	$T = T_w$	
B.C. 3	@ the inlet	$\forall r \wedge \forall t:$	$u = u_{in},$	$v = 0,$	$T = T_{in}$	
B.C. 4	@ the outlet	$\forall r \wedge \forall t:$	$\frac{\partial^2 u}{\partial z^2} = 0,$	$\frac{\partial^2 v}{\partial z^2} = 0,$	$\frac{\partial^2 T}{\partial z^2} = 0$	

Grid resolutions of 101×201 for the CFD code and 21×21 for radiation code were employed in the computations in r and z directions, respectively. The numerical calculations were performed for different values of wall temperature based conduction-to-radiation parameter, N_w ($= \frac{k\kappa}{\sigma T_w^3}$= 1.0, 0.1, 0.05, 0.02, 0.008, 0.005) as well as for *no radiation* case.

For varying values of conduction-to-radiation parameter, N_w, comparisons between the predictions of Baek *et al.* [31] and those of the present code for the radial

temperature profiles at $z/L = 0.5$ and the mixed mean temperature profiles along the pipe were illustrated in Figures 5.2 and 5.3, respectively. As can be seen from the figures, the predicted temperature profiles are in good agreement with the benchmark solution.

Also in the figures the effect of radiation on the temperature field was illustrated. As the conduction to radiation ratio decreases, the medium attain higher temperatures. From Figure 5.2 it can be seen that only for the cases of *no radiation* and $N_w = 1.0$, the centerline temperatures are approximately equal to the inlet temperatures. However as the value of conduction-to-radiation parameter, N_w, decreases, centerline temperatures reach much higher values due to the far-reaching effect of radiation emanating from hot walls. Furthermore, for the pipe length under consideration mixed mean temperature of the medium can reach a constant value when $N_w = 0.02$, $N_w = 0.008$ and $N_w = 0.005$ as depicted by Figure 5.3. This indicates that fully developed conditions can only be observed for the abovementioned cases.

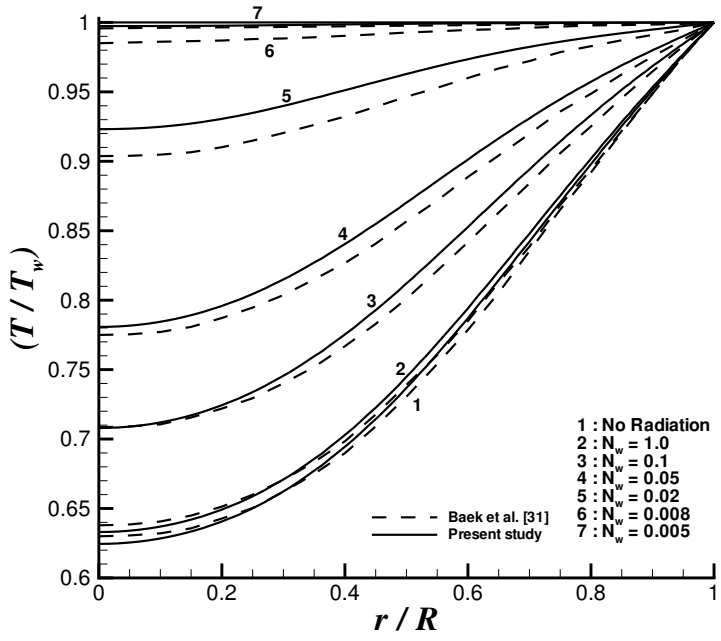

Figure 5.2: Effect of the conduction-to-radiation parameter, N_w, on the radial temperature profile at $z/L = 0.5$.

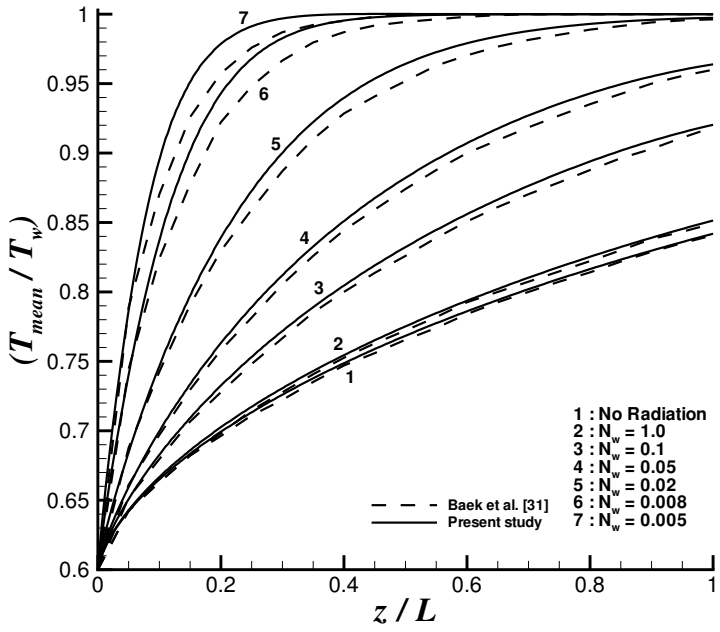

Figure 5.3: Effect of the conduction-to-radiation parameter, N_w, on the mixed mean temperature.

5.3 Test Case II: Validation of the Coupled Code for Thermally Radiating Turbulent Pipe Flow

The predictive accuracy of the coupled code for turbulent radiating flow was assessed on the test problem of Smith *et al.* [21]. The system under consideration consists of turbulent flow of a hot, radiatively absorbing, emitting gas through a black-walled circular pipe. The schematic representation of the system is illustrated in Figure 5.4. The aspect ratio of the system (D/L) is 0.2. The fluid enters the pipe with a fully

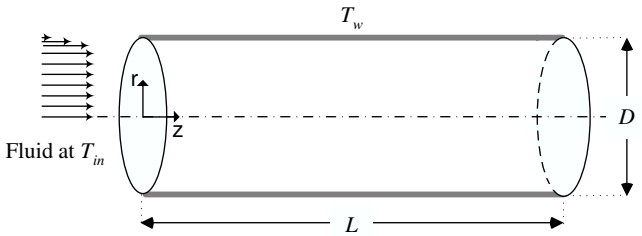

Figure 5.4: Schematic representation of the system.

developed turbulent velocity profile and uniform inlet temperature profile, T_{in}. The flow inside the pipe is hydrodynamically developed and turbulent. Moreover, the fluid exhibits constant thermophysical properties. The wall of the pipe is at constant temperature, T_w and the inlet to wall temperature ratio, (T_{in}/T_w) is 2.5. At the inlet and outlet of the pipe, radiatively black imaginary surfaces are assumed to exist. The inlet imaginary surface is assigned the inlet gas temperature and outlet imaginary surface is assumed at the outlet fluid bulk temperature. The Péclet number, *Pe* is equal to $10,000$ and the Prandtl number, *Pr* is 0.71. The axial conduction is negligible within the gas. The conduction-to-radiation parameter, $N_{ref}(=\frac{k}{\sigma T_{ref}^3})$ based on reference temperature is 0.01.

In the reference study [21], Smith *et al.* treated the medium as being both gray and non-gray. For gray treatment the calculations were performed for optically thin ($\tau_D = 0.1$), intermediately thick ($\tau_D = 1.0$), and thick ($\tau_D = 10.0$) mediums, whereas for non-gray treatment a real gas at a total pressure of 1.0 *atm* consisting of an equimolal mixture of carbon dioxide and water vapor both existing at a partial pressure of 0.1 *atm* was considered. For the prediction of the radiative properties of the medium the weighted sum of gray gases model was utilized. The results obtained by the authors point out that in terms of radiative properties the system can be reasonably described by a gray gas with $\tau_D = 0.1$. Having this in mind, the coupled code was executed for optically thin medium ($\tau_D = 0.1$) with the prescribed conditions. Grid independent solutions were obtained for the grid resolutions of 101×501 and 11×51 for CFD and radiation codes, respectively. The imposed initial and boundary conditions are tabulated in Table 5.2.

Figures 5.5-5.9 show the comparisons between the predictions of the present study and those of Smith *et al.* [21] for radial temperature profiles at different axial locations. As can be seen from the figures, the predicted temperature profiles are in good agreement with the numerical solution of Smith *et al.* [21] and the sharp temperature gradients occuring in the viscinity of the wall were well captured by the code.

Table 5.2: Initial & boundary conditions.

I.C.	@ $t = 0$	$\forall r \wedge \forall z:$	$u = 0,$	$v = 0,$	$T = T_{ref}$	$\vec{\nabla} \cdot \vec{q}_R = 0$
B.C. 1	@ the center	$\forall z \wedge \forall t:$	$\frac{\partial u}{\partial r} = 0,$	$v = 0,$	$\frac{\partial T}{\partial r} = 0$	
B.C. 2	@ the wall	$\forall z \wedge \forall t:$	$u = 0,$	$v = 0,$	$T = T_w$	
B.C. 3	@ the inlet	$\forall r \wedge \forall t:$	$u = u_{in},$	$v = 0,$	$T = T_{in}$	
B.C. 4	@ the outlet	$\forall r \wedge \forall t:$	$\frac{\partial^2 u}{\partial z^2} = 0,$	$\frac{\partial^2 v}{\partial z^2} = 0,$	$\frac{\partial^2 T}{\partial z^2} = 0$	

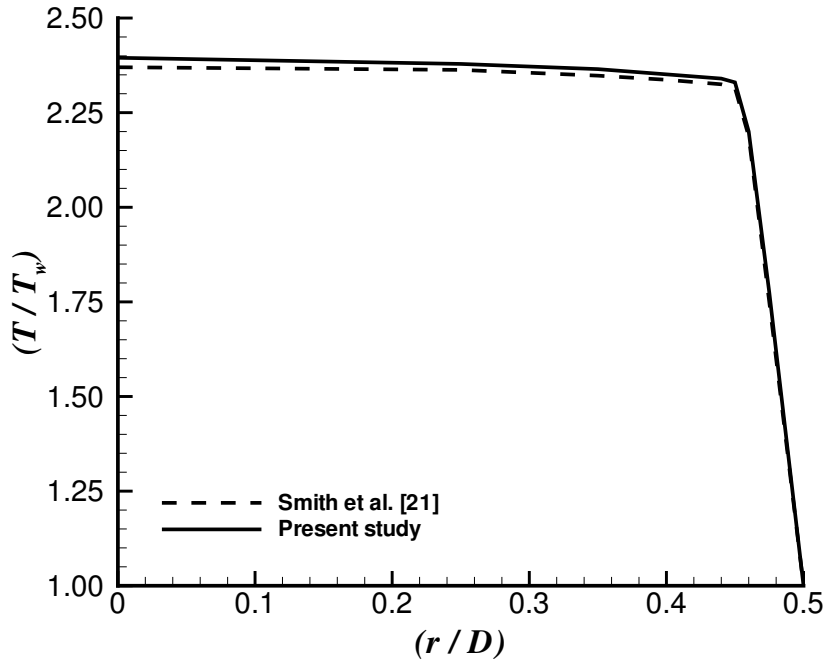

Figure 5.5: Radial temperature profile at z=80 *cm*.

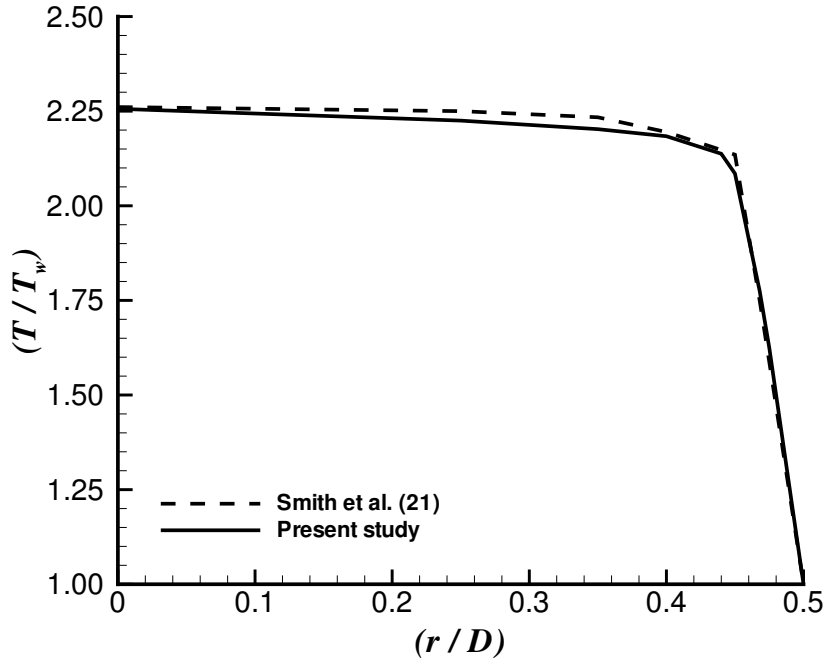

Figure 5.6: Radial temperature profile at z=180 *cm*.

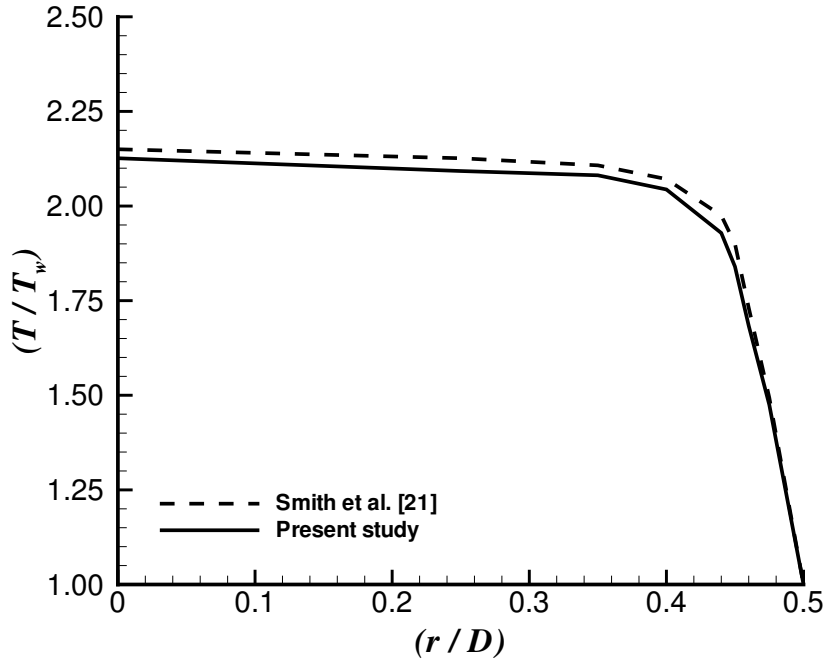

Figure 5.7: Radial temperature profile at z=280 *cm*.

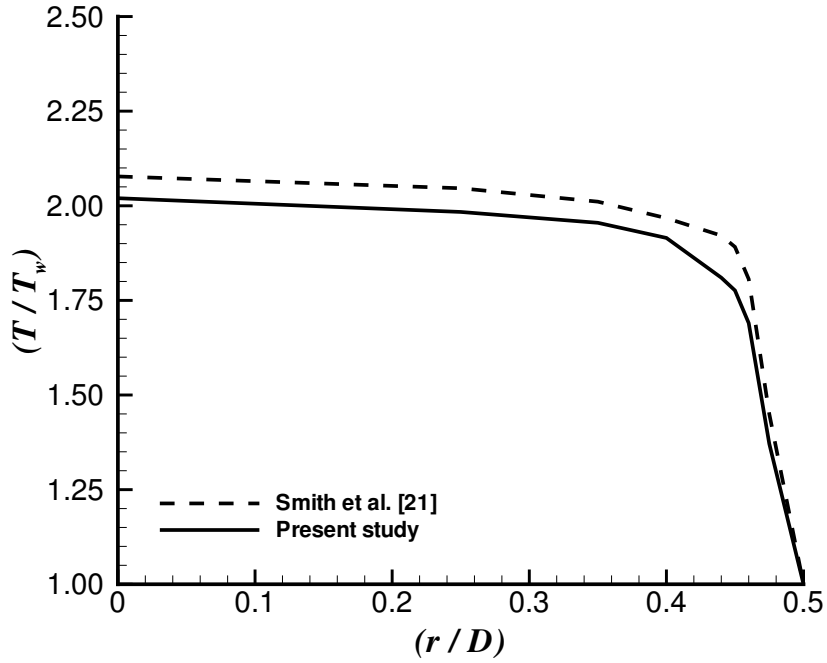

Figure 5.8: Radial temperature profile at z=380 *cm*.

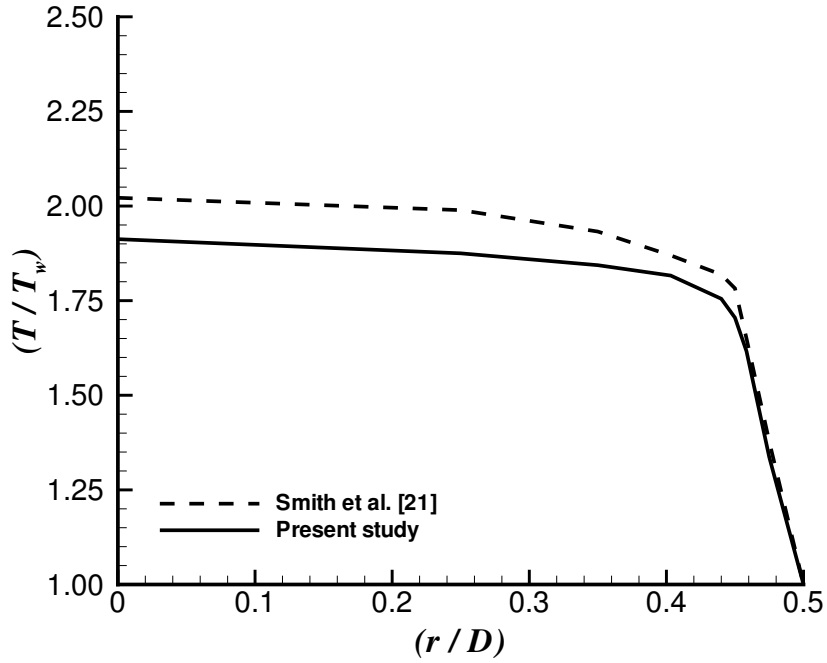

Figure 5.9: Radial temperature profile at z=500 *cm*.

5.4 Test Case III: Transient Simulation of Laminar/Turbulent, Radiating Flow of Carbon dioxide

Having validated the predictive accuracy of the coupled code for steady, laminar/turbulent, radiating pipe flows, the predictive performance of the code for the transient radiating flows is tested on the test problem described below.

The physical system under consideration consists of laminar/turbulent flow of carbon dioxide at atmospheric pressure through a black-walled circular pipe subject to an abrupt change of the wall temperature at the abscissa $z = l_0$. The diameter of the pipe D is 20 cm, and the solution domain in axial direction covers a region of 200 cm starting from 20 cm upstream from the temperature change point ($L = 200$ cm and $l_0 = 20$ cm). The schematic representation of the system is demonstrated in Figure 5.10. The wall temperature is T_{w1} (500 K) in the region upstream of the heating section $z \leq l_0$, and T_{w2} (1500 K) in the region downstream from the heating section $z > l_0$. The temperature dependence of the fluid thermophysical and radiative properties have been accounted for.

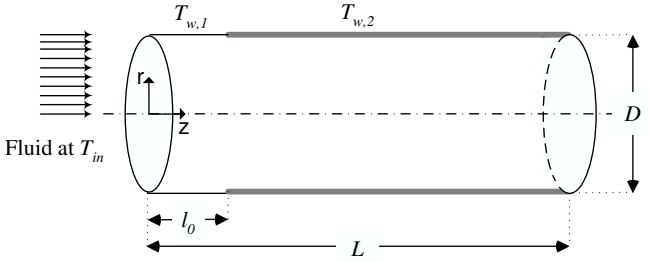

Figure 5.10: Schematic diagram of the system.

The numerical calculations were performed for two different Reynolds number of 2,000 and 10,000 based on the average velocity. The grid resolutions used in the simulations are 101×401 for the CFD code and 11×41 for the radiation code in r- and z-directions, respectively. The code was executed until steady-state on a single processor (Pentium III 1000MHz with 1000MB RAM).For Reynolds numbers of 2,000 and 10,000 the code used about 16.2 h ($t_{st} = 3.6$ s) and 6.5 h ($t_{st} = 1.6$ s) of CPU time, respectively.

The imposed initial and boundary conditions are tabulated in Table 5.3.

Table 5.3: Initial & boundary conditions.

I.C.	@ $t = 0$	$\forall r \wedge \forall z:$	$u = 0,$	$v = 0,$	$T = T_{ref}$	$\vec{\nabla} \cdot \vec{q}_R = 0$
B.C. 1	@ the center	$\forall z \wedge \forall t:$	$\frac{\partial u}{\partial r} = 0,$	$v = 0,$	$\frac{\partial T}{\partial r} = 0$	
B.C. 2	@ the wall	$\forall z \wedge \forall t:$	$u = 0,$	$v = 0,$	$T = T_w$	
B.C. 3	@ the inlet	$\forall r \wedge \forall t:$	$u = u_{in},$	$v = 0,$	$T = T_{in}$	
B.C. 4	@ the outlet	$\forall r \wedge \forall t:$	$\frac{\partial^2 u}{\partial z^2} = 0,$	$\frac{\partial^2 v}{\partial z^2} = 0,$	$\frac{\partial^2 T}{\partial z^2} = 0$	

Figures 5.11 and 5.12 illustrate from left to right, the time development of temperature (a), velocity (c) and radiative source term (c) fields for $Re = 2,000$ and $Re = 10,000$, respectively.

Examination of the temperature fields in Figure 5.11.(a) reveals that the temperature of the medium increases rapidly with time due to pronounced effect of radiation emanating from the hot wall. At $t = 2.4\ s$ and $z > 130$ the medium temperature reaches the wall temperature. Also, as can be seen from the figure, the temperature in the upstream region of heating section $(z < l_0)$ increases due to axial propagation of radiation.

Inspection of the corresponding velocity fields in Figure 5.11.(b) shows an acceleration in the flow with time due to increasing medium temperature. As can be seen from the figure the velocity and temperature wave fronts propagate simultaneously.

The time development of radiative energy source term field is illustrated in Figure 5.11(c). The radiative energy source term corresponds to the difference between the emitted and absorbed energies. Therefore it is directly influenced by the temperature field. Since the temperature of the medium decreases from the wall to the centerline, the emitted energy also decreases and this leads to a decrease in radiative energy source terms.

Figure 5.12 illustrates the time development of above mentioned variables for $Re = 10,000$ case. As can be seen from Figure 5.12.(a), the heat released from the wall can penetrate only a small portion towards the center for this case. A comparison between the $Re = 2,000$ and $Re = 10,000$ cases reveals that upstream propagation of radiation observed for the $Re = 10,000$ case is not as pronounced as that for the $Re = 2,000$ case due to high velocity flow.

Figure 5.12.(b) illustrates the time development of velocity field for $Re = 10,000$ case. When the figure is inspected, it is seen that with the effect of radiation the near wall region heats up rapidly resulting in a decrease in the density. Although it is expected to obtain relatively lower velocities in this region, the decrease in the density counterbalances viscous forces and results in higher velocities than that observed in a typical convection dominated turbulent flow.

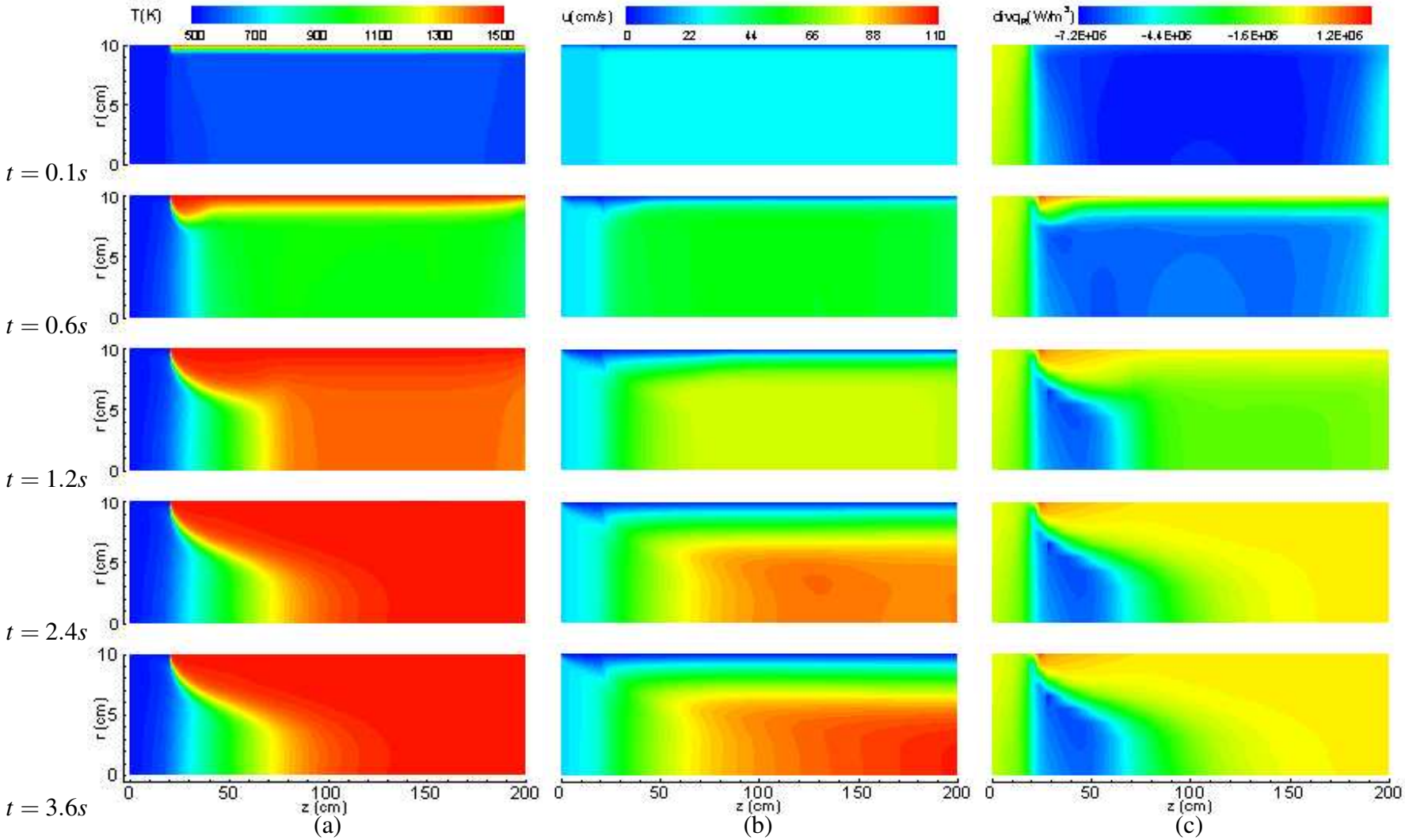

Figure 5.11: Time development of temperature (a), velocity (b) and radiative energy source term (c) fields at $Re = 2,000$.

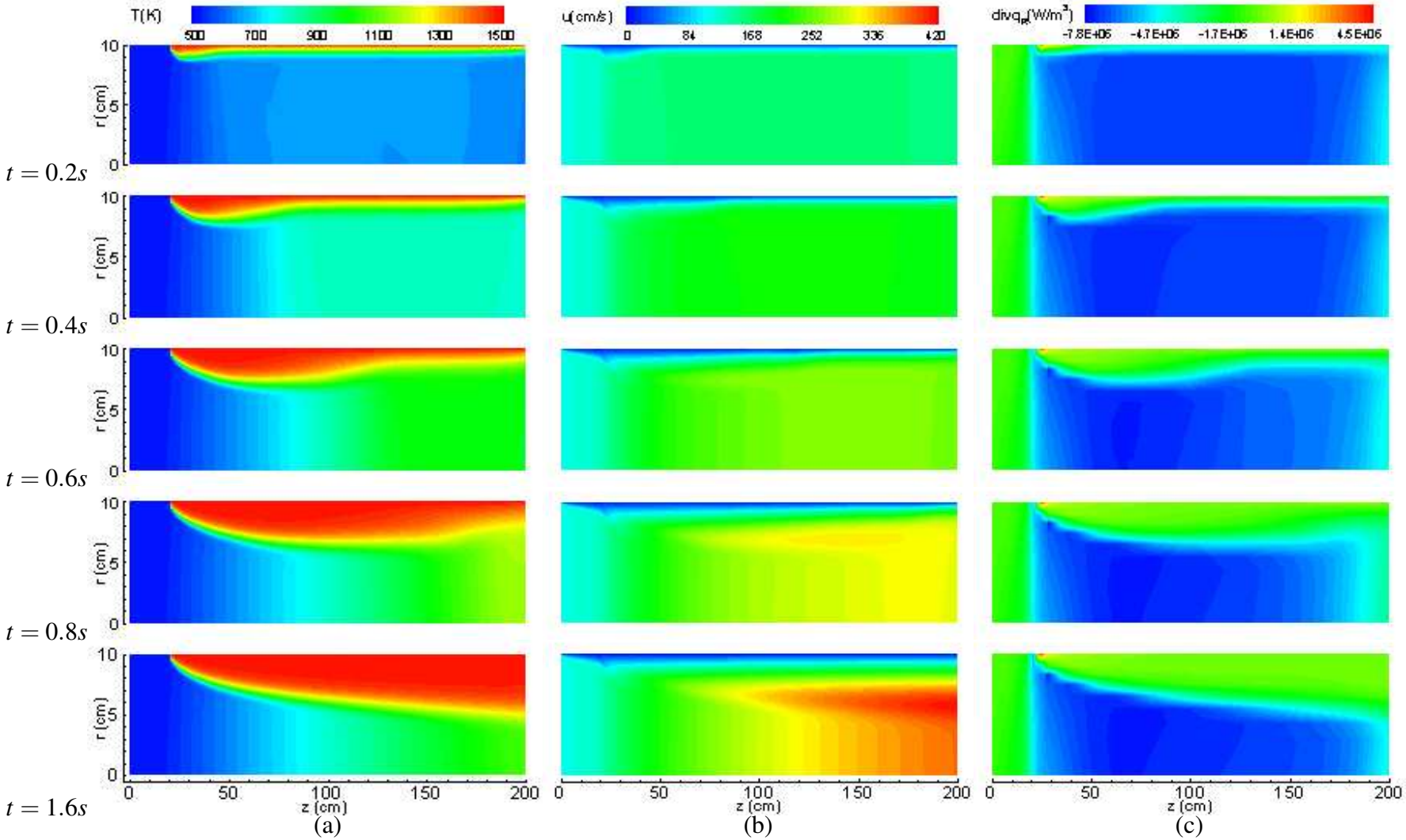

Figure 5.12: Time development of temperature (a), velocity (b) and radiative energy source term (c) fields at $Re = 10,000$.

5.5 Performance of the Parallel Code

The simulations carried out by sequential and parallel codes show that parallel code reproduces the same results with the sequential code. The performance of the sequential and parallel codes was investigated by examining two performance criteria, speed-up and efficiency. For comparative purposes, computations were carried out for the Re=10,000 case of Test Case III using the same grids and time steps and final time. The execution was performed on a parallel cluster which consists of

- 1 dual processor PC with 1000MB RAM (Pentium III 1000MHz)
- 1 dual processor PC with 512MB RAM (Pentium III 700MHz)

running on Red Hat Linux 7.3 with Open Mosix kernel (2.4.22) connected via 10/100Mbps switch.

For the same conditions stated above the parallel code was found to use about 2.1 h of CPU time whereas the sequential code had used 6.5 h. Based on this values the speed-up and efficiency values were calculated as 3.1, and 77%, respectively.

CHAPTER 6

CONCLUSIONS

Predictive accuracy of the previously developed coupled code was tested by applying it to the prediction of heat transfer and flow characteristics in thermally radiating laminar/turbulent flow of gray gases through axisymmetric cylindrical geometries, and validated by comparing its steady-state predictions with the numerical solutions available in the literature. Having validated the predictive accuracy of the coupled code for steady laminar/turbulent radiating pipe flows, the performance of the code for transient radiating flows was tested on a more realistic test problem involving laminar/turbulent flow of carbon dioxide through a circular pipe. Based on the numerical experimentations, the following conclusions are reached.

- The coupled code is able to produce accurate results for laminar pipe flow of gray gases in the presence of weak, moderate or strong thermal radiation.
- For laminar conditions the effect of radiation on the temperature field is more pronounced than that in turbulent conditions.
- The coupled code can produce accurate results for turbulent conditions.
- Parallelization is a useful tool for reducing the CPU time.

6.1 Suggestions for Future Work

Based on the experience gained in the numerical experimentation, the following recommendations for future extension of the work are suggested.

- As turbulence is a three-dimensional phenomena, for more accurate DNS applications three-dimensional formulation of the code is required.

- Accurate calculation of the radiative energy source terms must include the effects of turbulent fluctuations, hence the coupling of nonlinear turbulence effects is particularly important.
- Since the radiative properties of a medium depends on wavelength, a non-gray radiation model can be developed and incorporated into the coupled code.

REFERENCES

[1] R. Viskanta, "Interaction of heat transfer by conduction, convection, and radiation in a radiating fluid", *ASME Journal of Heat Transfer*, 1963.

[2] R. Viskanta, "Heat transfer in a radiating fluid with slug flow in a parallel plate channel", *Applied Scientific Research, Sec A*, vol. 13, pp. 291–311, 1964.

[3] D. K. Edwards and A. Balakrishnan, "Nongray radiative transfer in a turbulent gas layer", *Int. J. Heat Mass Transfer*, vol. 16, pp. 1003–1015, 1973.

[4] A. Balakrishnan and D. K. Edwards, "Established laminar and turbulent channel flow of a radiating molecular gas", *Heat Transfer*, vol. 1, pp. 93–97, 1974.

[5] A. T. Wassel and D. K. Edwards, "Molecular gas radiation in a laminar or turbulent pipe flow", *Journal of Heat Transfer*, vol. 98 Ser C, no. 1, pp. 101–107, 1976.

[6] C. C. Lii and M. N. Özisik, "Heat transfer in an absorbing, emitting and scattering slug flow between parallel plates", No. ASME Paper No.73-HT-13, (Atlanta), ASME-AIChE Heat Transfer Conference, 1973.

[7] S. T. Liu and R. S. Thorsen, "Combined force convection and radiation heat transfer in the thermal entrance region of a non-isothermal parallel plate channel-optically thin gases", No. ASME Paper No.73-HT-14, (Atlanta), ASME-AIChE Heat Transfer Conference, 1973.

[8] B. E. Pearce and A. F. Emery, "Heat transfer by thermal radiation and laminar forced convection to an absorbing fluid in the entry region of a pipe", *ASME Journal of Heat Transfer*, vol. 92, no. 2, pp. 221–230, 1970.

[9] A. Balakrishnan and D. K. Edwards, "Molecular gas radiation in the thermal entrance region of a duct", *Journal of Heat transfer*, vol. 101, pp. 489–495, 1979.

[10] T. C. Chawla and S. H. Chan, "Combined radiation convection in thermally developing poiseuille flow with scattering", *Journal of Heat Transfer*, vol. 102, no. 2, pp. 297–302, 1980.

[11] Y. Kurosaki, "Heat transfer by radiation and other transport mechanisms", *Bulletin of the JSME*, vol. 14, pp. 572–580, 1971.

[12] H. Tamehiro, R. Echigo, and S. Hasegawa, "Radiative heat transfer by flowing multiphase medium-iii. an analysis on heat transfer of turbulent flow in a circular tube", *Int. J. Heat Mass Transfer*, vol. 16, pp. 1199–1213, 1973.

[13] F. H. Azad and M. F. Modest, "Combined radiation and convection in absorbing, emitting and anisotropically scattering gas-particulate tube flow", *Int. J. Heat Mass Transfer*, vol. 24, no. 10, pp. 1681–1698, 1981.

[14] A. M. Al-Turki and T. F. Smith, "Radiative and convective transfer in a cylindrical enclosure for a gas/soot mixture", *Journal of Heat Transfer*, vol. 109, no. 1, pp. 259–262, 1987.

[15] S. Tabanfar and M. F. Modest, "Combined radiation and convection in absorbing, emitting nongray gas-particulate tube flow", *Journal of Heat Transfer - Transactions of ASME*, vol. 109, pp. 478–484, 1987.

[16] T. J. Chung and J. Y. Kim, "Two-dimensional, combined-mode heat transfer by conduction, convection, and radiation in emitting, absorbing and scattering media-solution by finite elements", *Journal of Heat Transfer*, vol. 106, pp. 448–452, 1984.

[17] M. Kassemi and B. T. F. Chung, "Two-dimensional convection and radiation with scattering from a poiseuille flow", *Journal of Thermophysics and Heat Transfer*, vol. 4, no. 1, pp. 98–105, 1990.

[18] R. Echigo, S. Hasegawa, and K. Kamiuto, "Composite heat transfer in a pipe with thermal radiation of two-dimensional propagation - in connection with the temperature rise in flowing medium upstream from heating section", *Int. J. Heat Mass Transfer*, vol. 18, no. 10, pp. 1149–1159, 1975.

[19] J. M. Huang and J. D. Lin, "Combined radiative and forced convective heat transfer in thermally-developing laminar flow through a circular pipe," *Chem. Eng. Comm. 1991*, vol. 101, pp. 147–164, 1991.

[20] T. H. Einstein, "Radiant heat transfer to absorbing gases enclosed in a circular pipe with conduction, gas flow, and internal heat generation", Tech. Rep. Rept. TR R-156, NASA Rept. TR R-156, 1963.

[21] T. F. Smith, Z. F. Shen, and A. M. Alturki, "Radiative and convective transfer in

a cylindrical enclosure for a real gas", *Journal of Heat Transfer*, vol. 107, no. 2, pp. 482–485, 1985.

[22] T. F. Smith, K. Byun, and M. J. Ford, "Heat transfer for flow of an absorbing, emitting, and isotropically scattering medium through a tube with reflecting walls", in *Proceedings of the International Heat Transfer Conference*, vol. 2, pp. 803–808, 1986.

[23] C. Schuler and A. Campo, "Numerical prediction of turbulent heat transfer in gas pipe flows subject to combined convection and radiation", *International Journal of Heat and Fluid Flow*, vol. 9, no. 3, pp. 308–315, 1988.

[24] T. Seo, D. A. Kaminski, and M. K. Jensen, "Combined convection and radiation in simultaneously developing flow and heat transfer with nongray gas mixtures", *Numerical Heat Transfer; Part A: Applications*, vol. 26, no. 1, pp. 49–66, 1994.

[25] C. W. Clausen and T. F. Smith, "Radiative and convective transfer for real gas flow through a tube with specified wall heat flux", *Journal of Heat Transfer*, vol. 101, no. 2, pp. 376–378, 1979.

[26] J. Stasiek, "Transformational-zone method of calculation of complex heat exchange during flow of optically active medium inside tube of diffuse grey surface", *Warme- und Stoffubertragung Zeitschrift*, vol. 22, no. 3-4, pp. 129–139, 1988.

[27] J. Stasiek and M. W. Collins, "Radiant and convective heat transfer for flow of a radiation gas in a heated/cooled tube with a grey wall", *International Journal of Heat and Mass Transfer*, vol. 36, no. 14, pp. 3633–3645, 1993.

[28] F. H. R. França and L. Goldstein, "Effects of temperature and geometry on the heat transfer from turbulent flow of a participating gas through a duct", *Heat Transfer Engineering*, vol. 19, no. 1, pp. 25–33, 1998.

[29] L. D. Nichols, "Temperature profile in the entrance region of an annular passage considering the effects of turbulent convection and radiation", *Int. J. Heat Mass Transfer*, vol. 8, pp. 589–607, 1965.

[30] S. DeSoto, "Coupled radiation, conduction and convection in entrance region flow", *Int. J. Heat Mass Transfer*, vol. 11, pp. 39–53, 1968.

[31] S. W. Baek, M. J. Yu, and T. Y. Kim, "Thermally developing poiseuille flow affected by radiation", *Numerical Heat Transfer; Part A: Applications*, vol. 35, no. 6, pp. 681–694, 1999.

[32] R. C. H. Tsou and C. S. Kang, "Upstream radiation effect to turbulent flow heat transfer in a tube", *Lett. Heat Mass Transfer*, vol. 3, no. 3, pp. 231–238, 1976.

[33] C. S. Landram, R. Greif, and I. S. Habib, "Heat transfer in turbulent pipe flow with optically thin radiation", *ASME J. Heat Transfer*, vol. 91, pp. 330–336, 1969.

[34] Z. Chiba and R. Greif, "Heat transfer to steam flowing turbulently in a pipe", *Int. J. Heat Mass Transfer*, vol. 16, pp. 1645–1648, 1973.

[35] C. K. Krishnaprakas, K. B. Narayana, and P. Dutta, "Combined convective and radiative heat transfer in turbulent pipe flow", *J. Thermophysics*, vol. 13, no. 3, pp. 390–394, 1999.

[36] F. B. Cheung, S. H. Chan, T. C. Chawla, and D. H. Cho, "Radiative heat transfer in a heat generating and turbulently convecting fluid layer", *Int. J. Heat Mass Transfer*, vol. 23, pp. 1313–1324, 1980.

[37] I. S. Habib and R. Greif, "Heat transfer to a flowing non-gray radiating gas: An experimental and theoretical study", *Int. J. Heat Mass Transfer*, vol. 13, pp. 1571–1582, 1970.

[38] A. T. Wassel, D. K. Edwards, and I. Catton, "Molecular gas radiation and laminar or turbulent heat diffusion in a cylinder with internal heat generation", *Int. J. Heat Mass Transfer*, vol. 18, pp. 1267–1276, 1975.

[39] N. K. Nakra and T. F. Smith, "Combined radiation-convection for a real gas", *ASME Journal of Heat Transfer*, vol. 99, pp. 60–65, 1977.

[40] Y. Yener and M. N. Özisik, "Simultaneous radiation and forced convection in thermally developing turbulent flow through a parallel-plate channel", *Journal of Heat Transfer*, pp. 985–988, 1986.

[41] A. Soufiani and J. Taine, "Application of statistical narrow-band model to coupled radiation and convection at high temperature", *Int. J. Heat Mass Transfer*, vol. 30, no. 3, pp. 437–447, 1987.

[42] A. Soufiani and J. Taine, "Experimental and theoretical studies of combined radiative and convective transfer in co_2 and h_2o laminar flows", *Int. J. Heat Mass Transfer*, vol. 32, no. 3, pp. 477–486, 1989.

[43] E. Sediki, A. Soufiani, and M. S. Sifaoui, "Spectrally correlated radiation and

laminar forced convection in the entrance region of a circular duct", *Int. J. of Heat Mass Transfer*, vol. 45, no. 25, pp. 5069–5081, 2002.

[44] N. Selçuk, A. B. Uygur, I. Ayranci, and T. Tarhan, "Transient simulation of radiating flows", *Journal of Quantitative Spectroscopy and Radiative Transfer*, vol. 93, no. 1-3, pp. 151–161, 2005.

[45] O. Oymak and N. Selçuk, "Method of lines solution of time-dependent two-dimensional Navier-Stokes equations", *Int. J. Numer. Meth. Fluids*, vol. 23, pp. 455–466, 1996.

[46] O. Oymak and N. Selçuk, "Transient simulation of internal separated flows using an intelligent higher-order spatial discretization scheme", *Int. J. Numer. Meth. Fluids*, vol. 24, pp. 759–769, 1997.

[47] O. Oymak, *Method of Lines Solution of Time–Dependent 2D Navier–Stokes Equations for Incompressible Separated Flows*, PhD thesis, Chemical Engineering department, M.E.T.U., Turkey, 1997.

[48] N. Selçuk and O. Oymak, "A novel code for the prediction of transient flow field in a gas turbine combustor simulator", in *Fuels*, pp. 11/1–10, 1999.

[49] T. Tarhan and N. Selçuk, "Method of lines for transient flow fields", *Int. J. Comp. Fluid Dyn.*, vol. 15, pp. 309–328, 2001.

[50] C. Ersahin, T. Tarhan, I. H. Tuncer, and N. Selçuk, "Parallelization of a transient navier-stokes code based on method of lines solution", *Int. J. Comp. Fluid Dyn.*, vol. 18, pp. 81–92, 2004.

[51] A. B. Uygur, T. Tarhan, and N. Selçuk, "Mol solution for transient turbulent flow in a heated pipe", *International Journal of Thermal Sciences*, vol. 44, no. 8, pp. 726–734, 2005.

[52] N. Selçuk and G. Kirbas, "The method of lines solution of discrete ordinates method for radiative heat transfer in enclosures", *Numer. Heat Trans., PART B*, vol. 37, pp. 379–392, 2000.

[53] N. Selçuk, A. Batu, and I. Ayranci, "Performance of method of lines solution of discrete ordinates method in the freeboard of a bubbling fluidized bed combustor", *Journal of Quantitative Spectroscopy and Radiative Transfer*, vol. 37, pp. 379–392, 2002.

[54] N. Selçuk and I. Ayranci, "The method of lines solution of the discrete ordinates method for radiative heat transfer in enclosures containing scattering media", *Numerical Heat Transfer B-Fundamentals*, vol. 43, no. 2, pp. 179–201, 2003.

[55] S. Harmandar and N. Selçuk, "The method of lines solution of discrete ordinates method for radiative heat transfer in cylindrical enclosures", *Journal of Quantitative Spectroscopy and Radiative Transfer*, vol. 84, pp. 395–407, 2004.

[56] I. Ayranci and N. Selçuk, "Mol solution of dom for transient radiative transfer in 3-d scattering media", *Journal of Quantitative Spectroscopy and Radiative Transfer*, vol. 84, pp. 409–422, 2004.

[57] R. B. Bird, W. E. Stewart, and E. N. Lightfoot, *Transport Phenomena* New York: John Wiley and Sons, 1960.

[58] X. S. Bai and L. Fuchs, "Modeling of turbulent reacting flows past a bluff body: Assessment of accuracy and efficiency", *Comput. Fluids*, vol. 23, pp. 507–521, 1994.

[59] Y. E. Egorov, A. E. Kuznetsov, M. K. Strelets, and M. L. Shur, "Subsonic compressible flows of chemically reacting gas mixtures in cylindrical and rectangular channels with sudden expansion", *Templofizika Vysokikh Temperatur*, vol. 28, no. 6, pp. 1149–1155, 1990.

[60] R. Siegel and J. R. Howell, *Thermal Radiation Heat Transfer* New York: McGraw-Hill, Inc., 1972.

[61] M. N. Özisik, *Radiative Transfer*, New York: John Wiley and Sons, 1973.

[62] M. F. Modest, *Radiative Heat Transfer*, New York: McGraw-Hill, Inc., 1993.

[63] W. E. Schiesser, *The Numerical Method of Lines: Integration of Partial Differential Equations*, New York: Academic press, 1991.

[64] N. Selçuk, G. Kirbas, and T. Tarhan, "Evaluation of method-of-lines solution of discrete ordinates method and finite volume method in a planar medium", in *Proceedings of the International Conference on Computational Heat and Mass Transfer (CHMT-99)*, (G. Magusa), pp. 358–366, 1999.

[65] T. Tarhan, *Numerical Simulation of Laminar Reacting Flows*, PhD thesis, Chemical Engineering department, M.E.T.U., Turkey, 2004.

[66] C. Hirsch, *Numerical Computation of Internal and External Flows; vol. 2: Computational Methods for Inviscid and Viscous Flows*, Chichester: John Wiley and Sons, 1998.

[67] G. D. Raithby and G. E. Schneider, "Numerical solution of problems in incompressible fluid flow", *Numer. Heat Transfer*, vol. 2, pp. 417–440, 1979.

[68] S. V. Patankar, "A calculation procedure for heat, mass and momentum transfer in three-dimensional parabolic flows", *Int. J. heat Mass Transfer*, vol. 15, p. 1787, 1806 1972.

[69] P. N. Brown, G. D. Byrne, and A. C. Hindmarsh, "Vode: A variable coefficient ode solver", *SIAM J. Sci. Stat. Comput.*, vol. 10, pp. 1038–1051, 1989.

[70] K. Radhakrishnan and A. C. Hindmarsh, "Description and use of lsode, the livermore solver for ordinary differential equations", Tech. Rep. UCRL-ID-113855, Lawrence Livermore National Laboratory, NASA, 1993.

[71] R. Weiner, B. A. Schmitt, and H. Podhaisky, "Rowmap - a row-code with krylov techniques for large stiff odes", Tech. Rep. 39, FB Mathematik und Informatik, Universitaet Halle, 1996.

[72] B. G. Carlson and K. D. Lathrop, "Transport theory- the method of discrete ordinates in computing methods in reactor physics", (New York), Gordon and Breach, 1968.

[73] J. Hyde and J. S. Truelove, "The discrete ordinates approximation for multidimensional radiant heat transfer in furnaces", Tech. Rep. HTFS-RS-189, AERE-R8502, AERE Harwell, 1977.

[74] A. Yücel, "Solution of the discrete ordinates equations for a radiatively participating medium by the method of lines", *Advances in Computer Methods for Partial Differential Equations VII*, pp. 838–844, 1992.

[75] N. Selçuk and N. Kayakol, "Evaluation of angular quadrature and spatial differencing schemes for discrete ordinates method in rectangular furnaces", in *Proc. of 31st National Heat Transfer Conference*, vol. 325, (Houston-Texas), pp. 151–158, ASME HDT, 1996.

[76] R. J. Kee, F. M. Rupley, E. Meeks, and J. A. Miller, "Chemkin-iii: a fortran chemical kinetics package for the analysis of gas-phasechemical and plasma kinetics", Tech. Rep. SAND96-8216, Sandia Laboratories, 1996.

[77] R. J. Kee, G. Dixon-Lewis, J. Warnatz, M. E. Coltrin, and J. A. Miller, "A fortran computer code package for the evaluation of the gas-phase, multicomponent transport properties", Tech. Rep. SAND86-8646, Sandia Laboratories, 1986.

[78] B. Leckner, "Spectral and total emissivity of water vapor and carbon dioxide", *Combust. Flame*, vol. 19, pp. 33–48, 1978.

[79] C. M. Bergman and J. B. Vos, "Parallelization of cfd codes", *Computer Methods in Applied Mechanics and Engineering*, vol. 89, pp. 523–528, 1991.

[80] B. Wilkinson and M. Allen, *Parallel Programming-Techniques and Applications Using Networked Workstations and Parallel Computers*, New Jersey: Prentice Hall Inc., 1999.

[81] G. R. Desrochers, *Principles of Parallel and Multi-Processing*, New York: McGraw-Hill, 1987.

APPENDIX A

ORDINATES AND WEIGHTS FOR S_N APPROXIMATIONS

Table A.1: Discrete ordinates for the S_N approximation for axisymmetric cylindrical geometry.

Order of approximation	Ordinates			Weights
	μ_m	η_m	ξ_m	w_m
S_2	0.5000000	0.7071068	0.5000000	3.1415927
S_4	0.2958759	0.2958759	0.9082483	1.0471976
	0.2958759	0.9082483	0.2958759	1.0471976
	0.9082483	0.2958759	0.2958759	1.0471976
S_6	0.1838670	0.1838670	0.9656013	0.3219034
	0.1838670	0.6950514	0.6950514	0.7252938
	0.6950514	0.1838670	0.6950514	0.7252938
	0.1838670	0.9656013	0.1838670	0.3219034
	0.6950514	0.6950514	0.1838670	0.7252938
	0.9656013	0.1838670	0.1838670	0.3219034
S_8	0.1422555	0.1422555	0.9795543	0.3424718
	0.1422555	0.5773503	0.8040087	0.1984568
	0.5773503	0.1422555	0.8040087	0.1984568
	0.1422555	0.8040087	0.5773503	0.1984568
	0.5773503	0.5773503	0.5773503	0.9234358
	0.8040087	0.1422555	0.5773503	0.1984568
	0.1422555	0.9795543	0.1422555	0.3424718
	0.5773503	0.8040087	0.1422555	0.1984568
	0.8040087	0.5773503	0.1422555	0.1984568
	0.9795543	0.1422555	0.1422555	0.3424718

APPENDIX B

SOURCE CODE OF THE SEQUENTIAL PROGRAM

B.1 Program SEQUENTIAL

```
!************************************************************************
      program sequential
      use common_header
      implicit none
!************************************************************************
!...
!...  set the version of the program
      version = 1            !UNIX
!     version = 2            !DOS
!...  beginning of the program
      call cpu_time(timestart)
!...
!...  set working path
      call execution_directory
!...
!...  sequential code parameters
      nos     = 0
      nostype = 0
!...
!...  perform everything before time integration
      call initial
!...
!...  perform time integration
 100  call time_integration
!...
!...  check for the end of the run
      tout = time + delt
      if(time <= (tf-0.5d0*delt)) goto 100
!...
!...  end of the program
      call cpu_time(timeend)
!...
!...  write the cpu time
      cpu = (timeend - timestart)
      write(*,920) cpu
!...
!...  formats
  920 format (1x,'cpu of program  :',1f12.2)
!...
!************************************************************************
      end program sequential
!************************************************************************
```

APPENDIX C

SOURCE CODE OF THE PARALLEL PROGRAM

C.1 Program MASTER

```
!************************************************************************
      program master
      use master_and_slave_header
      use common_header
      implicit none
!************************************************************************
!...  set the type of the program
      version = 1                          !UNIX
!...
!...  beginning of the program master
      call cpu_time(timestart)
!...
!...  set working path
      call execution_directory
!...
!...  read input data from file 'data.in'
      call read_parameters
!...
!...  allocate the arrays used in master program
      call allocate_pvm
!...
!...  start pvm
!      call pvmfstartpvmd (start,2,info)
      write(*,912)
      write(*,901)
!...
!...
      call pvmfmytid(mytid)
      call pvmfspawn(pathmaster, pvmdefault,'*', ndomain, itids, info)
!...
!...  error check
      if (info .lt. ndomain) then
      write (*,902)
      write (*,903) info
      else
      write (*,904) info
      endif
      write (*,905) mytid
      nerror=0
!...
!...  spawn slaves
      do nos = 1, ndomain
      nostype = 2
      if (nos == 1      ) nostype = 1
      if (nos == ndomain) nostype = 3
      write (*,906) nos, itids(nos)
      call pvmfinitsend (1, info)
      call pvmfpack (integer4,  ndomain,       1, 1, info)
      call pvmfpack (integer4, itids(1), ndomain, 1, info)
      call pvmfpack (integer4,       lp,       1, 1, info)
      call pvmfpack (  string,     path,      lp, 1, info)
      call pvmfpack (integer4,      nos,       1, 1, info)
```

```
      call pvmfpack (integer4,  nostype,       1, 1, info)
      call pvmfsend (                 itids(nos), 1, info)
      enddo
!...
!...
      write (*,912)
      write (*,910)
      write (*,912)
      write (*,919) t0,tf,delt,nframe
!...
!...  receive the number of grid points from slaves
      do nos=1,ndomain
      call pvmfrecv (itids(nos),1, info)
      call pvmfunpack (integer4,     nostype, 1, 1, info)
      call pvmfunpack (integer4,        nz_1, 1, 1, info)
      call pvmfunpack (integer4,        nz_2, 1, 1, info)
      call pvmfunpack (integer4,        nz_3, 1, 1, info)
      call pvmfunpack (integer4,        nz_4, 1, 1, info)
      call pvmfunpack (integer4,        nz_5, 1, 1, info)
      call pvmfunpack (integer4,          nr, 1, 1, info)
      call pvmfunpack (integer4,          nz, 1, 1, info)
      call pvmfunpack (integer4,      nr_rad, 1, 1, info)
      call pvmfunpack (integer4,      nz_rad, 1, 1, info)
      call pvmfunpack (real8,         dstart, 1, 1, info)
      call pvmfunpack (real8,           dend, 1, 1, info)
      call pvmfunpack (real8,     dstart_rad, 1, 1, info)
      call pvmfunpack (real8,       dend_rad, 1, 1, info)
      write (*,912)
      write (*,913) nos, nostype
      write (*,912)
      write (*,914) nz_1
      write (*,915) nz_2
      write (*,916) nz_3
      write (*,928) nz_4
      write (*,929) nz_5
      write (*,917) nr
      write (*,918) nz
      if (icode == 1) then
      write (*,922) nr_rad
      write (*,923) nz_rad
      endif
      write (*,924) dstart
      write (*,925) dend
      if (icode == 1) then
      write (*,926) dstart_rad
      write (*,927) dend_rad
      endif

      if (nz_1 /= 0) n1  = nos
      if (nz_2 /= 0) n2  = nos
      if (nz_3 /= 0) n3  = nos
      if (nz_4 /= 0) n4  = nos
      if (nz_5 /= 0) n5  = nos
      if (nz   /= 0) nnz = nos
      enddo
      write (*,912)

!      write(*,*)'before unpack'
!...
!...  unpack the informations sent by slaves
1     do nos = 1, ndomain
      call pvmfrecv (itids(nos), 1, info)
      call pvmfunpack (real8,    time_nos(nos), 1, 1, info)
      if (mech_no >= 0) then
      call pvmfunpack (real8, x_ch4_1_nos(nos), 1, 1, info)
      call pvmfunpack (real8, x_ch4_2_nos(nos), 1, 1, info)
      call pvmfunpack (real8, x_ch4_3_nos(nos), 1, 1, info)
      endif
      call pvmfunpack (real8,     u_1_nos(nos), 1, 1, info)
      call pvmfunpack (real8,     u_2_nos(nos), 1, 1, info)
```

```
      call pvmfunpack (real8,     u_3_nos(nos), 1, 1, info)
      call pvmfunpack (real8,    u_nz_nos(nos), 1, 1, info)
      call pvmfunpack (real8,     t_1_nos(nos), 1, 1, info)
      call pvmfunpack (real8,     t_2_nos(nos), 1, 1, info)
      call pvmfunpack (real8,     t_3_nos(nos), 1, 1, info)
      call pvmfunpack (real8,    t_nz_nos(nos), 1, 1, info)
!      write (99,*) 'time =',time_nos(nos),nos
      enddo
!      write(*,*)'after unpack'
!...
!...
      if (mech_no == -1) then
      write(*,400)                                                          &
           time_nos(1)                                                      &
        ,      u_1_nos(n1)    , u_2_nos(n3)    ,u_3_nos(n5), u_nz_nos(nnz)  &
        ,      t_1_nos(n1)    , t_2_nos(n3)    ,t_3_nos(n5), t_nz_nos(nnz)
      endif
!...
      if (mech_no >= 0) then
      write(*,400)                                                          &
           time_nos(1)                                                      &
        ,  x_ch4_1_nos(n1), x_ch4_2_nos(n2),x_ch4_3_nos(n3)                 &
        ,      u_1_nos(n1)    , u_2_nos(n3)    ,u_3_nos(n5), u_nz_nos(nnz)  &
        ,      t_1_nos(n1)    , t_2_nos(n3)    ,t_3_nos(n5), t_nz_nos(nnz)
      endif
!...
!...  receive slave's cpu time at each time step
      do nos = 1, ndomain
      call pvmfrecv (itids(nos), 1, info)
      call pvmfunpack (real8, cpu_nos(nos), 1, 1, info)
      enddo
      cpu = cpu + maxval(cpu_nos)
!...
!...  check for the end of the run
      if(time_nos(1) <= (tf-0.5d0*delt)) goto 1
!...
!...  end of the program
      call cpu_time(timeend)
!...
!...  write the cpu time
      write (*,920) cpu
      cpu = (timeend - timestart)
      write (*,921) cpu
!...
!...  finish the program
      call pvmfexit (info)
      write (*,*) 'Program Ends!'
!...
!... formats
  100 format (10h zone   i=,i3,2h, ,6h    j=,i3,2h, ,10h f=point  )
  200 format (8e16.5)
  300 format (35e16.5)
  400 format (1f8.6,13f11.5)
  901 format (1x,'PVM started')
  902 format ('Error in spawning the tasks!')
  903 format ('Only ',I1,' task(s) is(are) spawned!')
  904 format (1x,I2,' tasks are spawned...')
  905 format (1x,'Task ID of master  :', I7)
  906 format (1x,'Task ID of slave',I2,' :', I7)
  910 format (1x,'time integration parameters:')
  911 format (1x,'domain',I2,' :','   delt= ',1f6.5,'   tf= ',1f6.4)
  912 format (1x,'======================================')
  913 format (1x,'*  domain',I2,'   (nostype:',I1,')','  *')
  914 format (1x,'nz 1                  :',I8)
  915 format (1x,'nz 2                  :',I8)
  916 format (1x,'nz 3                  :',I8)
  928 format (1x,'nz 4                  :',I8)
  929 format (1x,'nz 5                  :',I8)
  917 format (1x,'pts. in r dir. in flow :',I8)
  918 format (1x,'pts. in z dir. in flow :',I8)
```

```
  922 format (1x,'pts. in r dir. in rad. :',I8)
  923 format (1x,'pts. in z dir. in rad. :',I8)
  924 format (1x,'flow domain starts at  :',1f11.6)
  925 format (1x,'flow domain ends at    :',1f11.6)
  926 format (1x,'rad. domain starts at  :',1f11.6)
  927 format (1x,'rad. domain ends at    :',1f11.6)
  919 format (1x,'initial time           :',1f8.6/ &
              1x,'final time             :',1f8.6/ &
              1x,'time step              :',1f8.6/ &
              1x,'# of frame             :',I8)
  920 format (1x,'cpu of slaves          :',1f12.2)
  921 format (1x,'cpu of master          :',1f12.2)
!#########################################################################
      end program master
!#########################################################################
```

C.2 Program SLAVE

```
!########################################################################
      program slave
      use master_and_slave_header
      use common_header
      implicit none
!########################################################################
!...  set the type of the program
      version = 1                          !UNIX
!...
!...  start slave
      call pvmfparent (mtid)
      call pvmfmytid (mytid)
!...
!...  recieve task ID and nos info from master
      call pvmfrecv (mtid, 1, info)
      call pvmfunpack (integer4,     ndomain,    1, 1, info)
!...
!...  allocate the arrays used in master program
      call allocate_pvm
      call pvmfunpack (integer4, itids(1), ndomain, 1, info)
      call pvmfunpack (integer4,       lp,       1, 1, info)
      call pvmfunpack (  string,     path,      lp, 1, info)
      call pvmfunpack (integer4,      nos,       1, 1, info)
      call pvmfunpack (integer4,  nostype,       1, 1, info)
!...
!...  check for error
      if (nos .lt. 0) then
         nerror=-nos
         call pvmfexit (info)
         stop
      endif
!...
!...  perform everything before time integration
      call initial
!...
!...  send the number of grid points to master
      call pvmfinitsend (1, info)
      call pvmfpack (integer4,      nostype, 1, 1, info)
      call pvmfpack (integer4,         nz_1, 1, 1, info)
      call pvmfpack (integer4,         nz_2, 1, 1, info)
      call pvmfpack (integer4,         nz_3, 1, 1, info)
      call pvmfpack (integer4,         nz_4, 1, 1, info)
      call pvmfpack (integer4,         nz_5, 1, 1, info)
      call pvmfpack (integer4,           nr, 1, 1, info)
      call pvmfpack (integer4,           nz, 1, 1, info)
      call pvmfpack (integer4,       nr_rad, 1, 1, info)
      call pvmfpack (integer4,       nz_rad, 1, 1, info)
!...
!...  send the domain info to master
      call pvmfpack (real8,     domstr(nos), 1, 1, info)
      call pvmfpack (real8,     domend(nos), 1, 1, info)
      call pvmfpack (real8, domstr_rad(nos), 1, 1, info)
      call pvmfpack (real8, domend_rad(nos), 1, 1, info)
      call pvmfsend (mtid, 1, info)


!...
!...  beginning of the time integration
 100  continue
      call cpu_time(timestart)
!...
!...  perform time integration
      call time_integration
!...
!...  boundary exchange between the domains
      call boundary_transfer
```

```
!...  send information to master
      call pvmfinitsend (1, info)
      call pvmfpack (real8,          time, 1, 1, info)
      if (mech_no >= 1) then
      call pvmfpack (real8,x(ich4,1,nz_1), 1, 1, info)
      call pvmfpack (real8,x(ich4,1,nz_3), 1, 1, info)
      call pvmfpack (real8,x(ich4,1,nz_5), 1, 1, info)
      endif
      call pvmfpack (real8,     u(1,nz_1), 1, 1, info)
      call pvmfpack (real8,     u(1,nz_3), 1, 1, info)
      call pvmfpack (real8,     u(1,nz_5), 1, 1, info)
      call pvmfpack (real8,     u(1,nz  ), 1, 1, info)
      call pvmfpack (real8,     t(1,nz_1), 1, 1, info)
      call pvmfpack (real8,     t(1,nz_3), 1, 1, info)
      call pvmfpack (real8,     t(1,nz_5), 1, 1, info)
      call pvmfpack (real8,     t(1,nz  ), 1, 1, info)
      call pvmfsend (mtid, 1, info)
!...
!...  send cpu of slave
      call cpu_time(timeend)
      cpu     = (timeend-timestart)
      call pvmfinitsend (1, info)
      call pvmfpack (real8, cpu, 1, 1, info)
      call pvmfsend (mtid, 1, info)
!...
!...  check for the end of the run
      tout = time + delt
      if(time <= (tf-0.5d0*delt)) goto 100
!...
!...  end of the slave
      call pvmfexit (info)
!...
!#########################################################################
      end program slave
!#########################################################################
```